On the influence of sea-ice physics in multi-decadal ocean-ice hindcasts

Petteri Uotila[1], Dorotea Iovino[2], Martin Vancoppenolle[3], Mikko Lensu[1], and Clement Rousset[3]

[1]Finnish Meteorological Institute, Helsinki, Finland
[2]Fondazione Centro Euro-Mediterraneo sui Cambiamenti Climatici (CMCC), Bologna, Italy
[3]Sorbonne Universités (UPMC Paris 6), LOCEAN-IPSL, CNRS/IRD/MNHN, Paris, France

Correspondence to: Petteri Uotila (petteri.uotila@fmi.fi)

Abstract. A set of hindcast simulations with the new NEMO3.6 ocean-ice model in the ORCA1 grid and forced by the DFS5.2 atmospheric data was performed from 1958–2012. We focussed on simulations that differ only in their sea-ice component: the old standard version LIM2 and its successor LIM3. Main differences between these sea-ice models are the parameterisations of sub-grid-scale sea-ice thickness distribution, ice deformation, thermodynamic processes, and sea-ice salinity. Our main

5 objective was to diagnose the ocean-ice sensitivity to the updated NEMO-LIM sea-ice physics. Results of such analysis have not been published for this new NEMO version.

In the polar regions, NEMO-LIM3 compares better with observations, while NEMO-LIM2 deviates more, producing too much ice in the Arctic, for example. Differences between NEMO-LIM2 and NEMO-LIM3 do not change in simulations even when the freshwater adjustments are turned off. In the extra-polar regions, the oceanographic conditions of the two NEMO-

10 LIM versions remain relatively similar, although they slowly drift apart over decades. A simplified NEMO-LIM3 configuration, having a virtual, single-category sea-ice thickness distribution, produced sea ice with a skill sufficient for ocean-ice hindcasts that target oceanographic studies. We conclude that NEMO3.6 is ready to be used as a stand-alone ocean-ice model and as a component of coupled atmosphere-ocean models.

1 Introduction

15 Sea ice is an important part of Earth's climate system because it effectively regulates the amount of energy being transferred between the atmosphere and oceans (Vaughan et al., 2013). Our current understanding on sea-ice related climate dynamics is incorporated in complex yet realistic climate models consisting of a sea-ice model component which is coupled to atmospheric and oceanic components (Griffies, 2004). In these models, sea ice can affect the ocean circulation and hydrography through ocean-ice interactions (see for example, Goosse and Fichefet, 1999; Kjellsson, 2015). To understand the effect of sea ice on the

20 ocean, coupled global ocean-ice models, where the coupled atmospheric component is replaced with prescribed atmospheric forcing, can be used (Griffies et al., 2009).

Recently, the version 3.6 of the Nucleus for European Modelling of the Ocean (NEMO) was released, along with its new sea-ice component, Louvain-la-Neuve Sea Ice Model (LIM) version 3.6 (Madec et al., 2015; Rousset et al., 2015). The new LIM3 code implements many sea-ice physics improvements compared to the previous LIM2 code, as has already been documented

(Vancoppenolle et al., 2009b; Massonnet et al., 2011; Vancoppenolle et al., 2015). However, the effect of LIM3 on the ocean circulation and hydrography remain to be systematically investigated. Accordingly, our aim is to analyse NEMO-LIM2 and NEMO-LIM3 simulations, particularly their ocean circulation and hydrography differences. As these differences may emerge over multi-decadal time scales due to slow oceanic processes, we carry out multi-decadal hindcast simulations with prescribed

5 atmospheric forcing. This analysis assists us to comprehensively understand the oceanic response to the state-of-the-science sea-ice physics in multi-decadal ocean-ice hindcasts.

To support our task, a significant body of literature presenting ocean-ice model assessments provide us an important reference when carrying out our NEMO-LIM assessments. For example, papers of the CORE-II virtual special issue of the Ocean Modelling Journal, such as Danabasoglu et al. (2014, 2016); Downes et al. (2015); Farneti et al. (2015); Griffies et al. (2014);

10 Wang et al. (2016a, b), and of the ORA-IP special issue of the Climate Dynamics Journal, such as Chevallier et al. (2015), are particularly relevant for this study. As the majority of CORE-II and ORA-IP ocean model configurations, our grid configuration (ORCA1) does not resolve ocean eddies. In this coarse-resolution ocean-ice model category, the eddy transport of momentum and heat are parameterised, for instance. Our simulations also share the use of CORE bulk formulae with the CORE-II experiments (Large and Yeager, 2004).

15 In the polar context, which is the regional focus of our study, the most important CORE-II papers include Downes et al. (2015), where the Antarctic sea ice and Southern Ocean water masses are analysed, and Wang et al. (2016a, b) who investigated the Arctic sea ice and the Arctic Ocean freshwater. Recently, Chevallier et al. (2015) analysed the Arctic sea ice in a set of ocean reanalyses to assess how the assimilation of observations affects the sea-ice characteristics. In addition to observational data, we use these ocean-ice model assessments as a benchmark when analysing our simulation performance.

20 The paper is divided into six sections. Section 2 describes the two versions of the ocean-ice models, NEMO-LIM2 and NEMO-LIM3, their initial and boundary conditions, model input data and observational reference data. In Section 3, we present sea-ice related results of the reference LIM3 hindcast simulation in comparison with observations and the reference LIM2 hindcast. Section 4 presents results of the NEMO-LIM sensitivity simulations to test the robustness of LIM3 and LIM2 differences for surface freshwater adjustments. In section 4 we also assess how realistic sea ice a simplified LIM3 single-

25 category ice thickness parameterisation reproduces. In section 5 differences of the ocean characteristics between NEMO-LIM2 and NEMO-LIM3 are discussed. Finally, the most important findings are highlighted in the conclusion section.

2   Models and Methods

All simulations presented here are based on the version 3.6_STABLE (revision 5918, released on 26 November 2015) of the NEMO-LIM ocean-ice modelling system (Madec et al., 2015), in the ORCA1 configuration. In NEMO, the OPA ocean

30 component is coupled with the LIM sea-ice model. For almost a decade, LIM2 has been the reference NEMO sea-ice model (Fichefet and Morales Maqueda, 1997), but in June 2015, a new and more sophisticated version, LIM3.6, became available as the reference sea-ice model for NEMO3.6 (Rousset et al., 2015).

2.1 NEMO ocean component OPA

OPA is a finite difference, hydrostatic, primitive equation ocean general circulation model. Its vertical coordinate system is based on z^* levels with partial cell thicknesses allowed at the sea floor. The vertical mixing of tracers and momentum uses the turbulent kinetic energy scheme (Gaspar et al., 1990; Blanke and Delcluse, 1993). A quadratic bottom friction boundary condi-

5   tion is applied together with an advective and diffusive bottom boundary layer for temperature and salinity tracers (Beckmann and Haidvogel, 1993). The model uses a non-linear variable volume scheme for the free surface, and an energy-enstrophy conserving scheme for momentum advection. A no-slip boundary condition is applied on the momentum equations with the horizontal Laplacian momentum diffusion. The tracer equations in OPA use the TVD advection scheme by Zalesak (1979) with the Laplacian diffusion along isoneutral surfaces.

10   The simulations are performed on an ORCA-like global tripolar grid with 1° nominal horizontal resolution and 75 vertical levels. Additional refinement of the meridional grid down to 1/3° is present near the Equator. The minimum horizontal grid cell length is about 50 km in the Arctic Ocean and 40 km in the Antarctic region, while the vertical level thickness ranges from 1 m near the surface increasing to 200 m at the bottom.

2.2 NEMO sea-ice components LIM2 and LIM3

15   Our ocean-ice configurations only differ in their sea-ice component, all other experimental conditions being identical. We use the levitating sea-ice framework, following the convention of Campin et al. (2008): the growth and melt of ice impact the ocean mass and the salinity, but do not affect the pressure experienced by the ocean surface.

LIM2 (Fichefet and Morales Maqueda, 1997; Timmermann et al., 2005) is a sea-ice model in the line of the two-level model of Hibler (1979). It features: a single sea-ice category and open water represented using ice concentration; the Semtner

20   (1976) 3-layer thermodynamics with a virtual reservoir of shortwave radiation heat which parameterizes brine inclusions; the revisited C-grid elastic-viscous-plastic rheology of Bouillon et al. (2013); the second-order moment-conserving advection scheme of Prather (1986), plus a few extra parameterisations. LIM2 implements the snow-ice formation by infiltration and freezing of seawater into snow when deep enough. The effect of sub-grid-scale snow and ice thickness distributions is implicitly parameterised by enhancing the conduction of heat through the ice and by melting the ice laterally to account for thin ice

25   melting. The surface albedo depends on the state of the surface (frozen or melting), snow depth, and ice thickness following Shine and Henderson-Sellers (1985).

LIM3.6 (Vancoppenolle et al., 2009a; Rousset et al., 2015) is a sea-ice model in the line of the AIDJEX model, with multiple sea-ice categories (Coon et al., 1974; Thorndike et al., 1975). Multiple categories allow to resolve the intense growth and melt of thin ice, as well as the redistribution of thinner ice onto thicker ice due to ridging and rafting. LIM3 dynamics (advection and

30   rheology) are the same as in LIM2. Thermodynamics are multi-layer and include an explicit description of the effect of brine on the storage and conduction of heat (Bitz and Lipscomb, 1999), and a parameterization of brine drainage (Vancoppenolle et al., 2009a) that affects ocean-ice salt exchanges. The default NEMO3.6 configuration uses five ice thickness categories and

two vertical layers for thermodynamics. Alternatively, LIM3.6 (Rousset et al., 2015) can be run with a single sea-ice category, using two virtual ice thickness distribution parameterisations (enhanced conduction and thin ice melting).

2.3 Model input data

The NEMO model bathymetry is a combination of ETOPO1 Amante et al. (2009) in the open ocean, and GEBCO (IOC, 2003) in coastal regions. All the simulations were extended over the period 1958–2012 and forced by the DFS5.2 atmospheric data set, developed through the DRAKKAR consortium (Brodeau et al., 2010). This data set is based on satellite observations (monthly precipitations and daily radiative heat fluxes) and combined ERA-40 (before 31 December 2001) and ERA-Interim (from 2002 onward) meteorological reanalyses, and provides 6-hourly air temperature and humidity at the 2 m level, and wind velocity at the 10 m level (Uppala et al., 2005; Dee et al., 2011). Prescribed surface boundary conditions were calculated by using the CORE bulk formulae proposed by Large and Yeager (2004). As in Brodeau et al. (2010), simulations were forced with the monthly river run-off climatology based on Timmermann et al. (2009). The ocean and sea-ice models had a time step of 3600 s, which was also the interval when surface boundary conditions were updated.

As a standard practice in forced ocean-ice simulations, the mean sea level controls were used to prevent the unrealistic drift of the sea surface height due to freshwater boundary forcing distorted by errors in precipitation, evaporation and river runoff (Griffies et al., 2014). Specifically, this was done by setting values `nn_fwb=2` and `nn_ssr=.true.` in the NEMO namelist. The `nn_fwb` parameter is used to reset the freshwater budget, evaporation minus precipitation minus river runoff, and `nn_ssr` enables the restoring of sea-surface salinity (SSS). Following the default ORCA1 NEMO3.6 configuration, the SSS restoring rate was set to -100 $\mathrm{mm/day}$ towards the SSS of Polar Hydrographic Climatology version 3 (PHC3) created by Steele et al. (2001).

2.4 Experiments

NEMO-LIM simulations started from the state of no motion in January 1958, with initial conditions for ocean temperature and salinity derived from PHC3 (Steele et al., 2001), and ended in December 2012. We completed two reference simulations, one using NEMO-LIM3 and another one using NEMO-LIM2, with recommended settings. In both LIM configurations, the initial sea-ice thickness was set to 3.0 m where the sea surface temperature was below 0 °C. The initial snow thickness was set to 0.3 m in LIM3 for both hemispheres, while in LIM2 it was 0.5 m in the Northern Hemisphere (NH) and 0.1 m in the Southern Hemisphere (SH). For both simulations, the initial sea-ice concentration was set to 90%, except for LIM2 in the NH, where the initial sea-ice concentration was 95%. The ice strength parameter P^* was set to 2×10^4 (1×10^4) Nm^{-1} in LIM3 (LIM2), while the ocean-ice drag coefficient was 5.0×10^{-3} and the atmosphere-ice drag coefficient follows Large and Yeager (2009) in both models.

Differences between LIM2 and LIM3 initial sea-ice and ice dynamics parameter values originate from the fact that they are recommended values according to the default NEMO3.6 configuration. Instead of setting the LIM2 initial values and ice dynamics identical to LIM3, for example, we took the point of view that we compare two different sea-ice models, each with

its own specific and optimised tuning, and with no specific focus on ice dynamics. This is the point of view that was adopted by Massonnet et al. (2011) as well.

Even though the sea-ice initialisation differs slightly in terms of hemispheric snow thickness, it does not impact our results which focus on the last decade 45 years after the initialisation. The lower LIM2 ice strength P^*, however, has an impact

5 and results in weaker ice that deforms easier producing a larger sea-ice volume than would have obtained with the P^* value identical to LIM3. Importantly, a LIM2 model experiment with the LIM3 P^* value, produces a less realistically evolving Arctic sea-ice volume, with too thin winter sea ice in particular, than with the recommended value. Furthermore, the LIM2 model experiment with the LIM3 P^* value produced almost similar sea-ice extent and area than the LIM2 experiment with the default P^* value, indicating insignificant oceanic impacts. These findings further motivated us to carry out our LIM2 simulations with

10 the recommended default ice dynamics parameter values.

In addition to the two reference simulations, we carried out sensitivity simulations to determine how significant and systematic differences between LIM3 and LIM2 are. In these sensitivity simulations, processes related to ocean-ice interactions were regulated and adjusted. In this way, we were able to isolate the impacts of individual processes and quantify their significance. First, we switched NEMO-LIM3 into its single-category mode which employs a virtual ice thickness distribution parameter-

15 isation, which make the model simpler and computationally cheaper than with multiple categories. Then, instead of using a prognostic salinity profile, we set the LIM3 sea-ice salinity to a constant value of 4 ppm, similarly to LIM2. As a result of the single-category and constant sea-ice salinity, LIM3 is physically to a greater extent closer to LIM2, is computationally fast, but more realistic than LIM2, particularly in the Arctic, as we will show.

The second set of sensitivity experiments were performed to examine the impact of ocean surface boundary conditions

20 on ocean-ice properties, and therefore to see how robust our LIM3–LIM2 comparison results are. For this, we carried out NEMO-LIM2 and NEMO-LIM3 simulations where the mean sea level controls were switched off by setting `nn_fwb=0` and `nn_ssr=.false.` in the NEMO configuration namelist. After completing these NEMO-LIM2 and NEMO-LIM3 simulations without freshwater adjustments, we calculated and compared their differences to the corresponding ones based on the reference simulations where the freshwater controls were kept on.

25 ## 2.5 Reference data

When quantitatively assessing the modelled sea-ice and upper ocean realism, we included comparisons with satellite-based and reanalysis products of sea-ice concentration, thickness and velocity. Since 1979, space-borne passive microwave sensors have produced a nearly continuous and consistent record of ice concentration which provides a good basis for model validation. For sea-ice concentration we used the NOAA/NSIDC Climate Data Record of Passive Microwave Sea Ice Concentration,

30 Version 2 (Meier et al., 2013), which covers both polar regions at a 25 km grid cell size. The observed sea-ice extent data, which were based on satellite observed sea-ice concentrations, are the NSIDC Sea Ice Index (Fetterer et al., 2002). For sea-ice velocity analysis, the OSI-SAF product by Lavergne et al. (2010) was used. Sea-ice thickness and volume were compared with reanalyses from the Pan-Arctic Ice-Ocean Modeling and Assimilation System (PIOMAS) for the NH, and from the Global

Ice-Ocean Modeling and Assimilation System (GIOMAS) for the SH (Schweiger et al., 2011). It is worth noting that these ice thickness data are model products, not entirely based on observations and have significant uncertainties.

For hydrographic comparisons, we decided to use two observational data sets. First, we selected aforementioned PHC3, which is a global climatology with a combination of NODC's 1998 world climatology, the EWG Arctic Ocean Atlas, and

5 selected Canadian data provided by the Bedford Institute of Oceanography (Steele et al., 2001). PHC3 was updated with the Arctic Ocean temperature and salinity observations in 2005. Additionally, we used the most recent World Ocean Atlas 2013 (WOA13) (Boyer et al., 2013) averaged over the years 2005–2012. WOA13 lacks the Arctic observations included in PHC3, but has more recent observations elsewhere. Therefore, at least outside the Arctic Ocean, the WOA13 data temporally matches better with our NEMO-LIM comparison period of 2003–2012. As we will show in Section 5, WOA13 and PHC3 mainly

10 differ in terms of Arctic SSS, while otherwise climatological differences are relatively small from the NEMO-LIM assessment perspective. Notably, Wang et al. (2016b) used PHC3 in their ocean-ice model Arctic intercomparison study, and using PHC3 here as well makes qualitative comparisons of our results with theirs straightforward. Finally, PHC3 was used to determine the initial hydrographic conditions of our model simulations, and comparisons between 2003–2012 LIM3 climatology and PHC3 show how much our simulations diverged from their initial state in 45 years.

15 Modelled mixed layer depths (MLD) were compared with the observational climatology by de Boyer Montégut et al. (2004). It should be noted that observational uncertainties in the Arctic Ocean and in polar regions south of 55°S are particularly large due to a limited number of measurements. Hence, we concentrated in the North Atlantic and the Southern Ocean outside the regions of high uncertainty in our MLD comparisons.

3 Sea-ice results

20 In this section, we analyse how well LIM reproduces large-scale climatological sea-ice properties (ice areal coverage, volume and drift). In order to evaluate the new sea-ice model, we compare LIM3 results to satellite observations, reanalysis data and as well as to the equivalent LIM2 simulation. All mean fields are computed over the last decade of integration, from 2003 to 2012. As the LIM3 sea-ice properties have already been analysed by (Vancoppenolle et al., 2009b; Massonnet et al., 2011; Vancoppenolle et al., 2015) and our results agree rather well with theirs, we only shortly present our sea-ice findings and

25 merely focus on the sensitivity simulations and oceanographic analysis in the sections following this one.

3.1 Sea-ice concentration and extent

In the NH in September, the geographical distribution of LIM3 sea-ice concentration presents high values in the Canadian Arctic Archipelago with a realistic latitudinal decrease toward the Eurasian Arctic (Figure 1a). LIM3 tends to generally underestimate the ice concentration, by ~20% in the central Arctic to ~50% in the East Siberian Sea (Figure 1b), while the Laptev

30 and Kara Seas are almost ice-free (Figure 1a). This negative summer sea-ice concentration bias is linked to an underestimation of sea-ice thickness in those areas both in winter and summer. By contrast, too-large ice concentration is found in the Beaufort Sea (Figure 1b). Clearly the representation of ice concentration in the two models significantly differs in summer: LIM2 pro-

duces higher sea-ice concentration compared to LIM3 everywhere in the Arctic Ocean and their difference increases radially from the Canadian Arctic Archipelago toward the Eurasian Arctic (Figure 1c). LIM2 cannot reproduce the seasonal cycle of ice area in the Beaufort and East Siberian Seas toward the Bering Strait, where its sea ice, unrealistically, is rather uniform spatially with a too small open water fraction until a sharp transition to the ice edge.

5   Mean seasonal cycles of the modelled sea-ice extents are shown in Figures 2a and b together with the NSIDC observations, all averaged over the years 2003–2012. In the NH, the LIM3 sea-ice extent closely follows the observed data and represents a clear improvement compared to LIM2, particularly in summer (Figure 2a). The respective LIM2 values are too high. LIM2 does not manage to melt enough ice and systematically overestimates the NH sea-ice extent. On the contrary, the LIM3 multi-category sea-ice thickness distribution allows for larger rates of melting due to its thin ice categories compared to the single-category

10 LIM2, and enhances the seasonal cycle of sea-ice extent bringing it closer to observations.

Associated with the better mean seasonal cycle, the inter-annual time series of sea-ice extent is improved in LIM3 compared to LIM2 (Figure 2b). Both the maximum and minimum sea-ice extent are well reproduced by LIM3, as shown by the time series in Figure 2b that closely follow the NSIDC data in 1979–2012. Moreover, LIM3 realistically captures most of the summer minimum extends, including the 2007 record minimum. In contrast, LIM2 systematically overestimates yearly minimum,

15 maximum and mean sea-ice extents during the whole period of integration. For example the 2007 minimum is overestimated by 50%. The two LIM models show comparable negative sea-ice extent trends in March, which are less negative than satellite observed trends. In September, the LIM3 trend is close to the observed one, while the LIM2 negative trend is too small. As concluded by Wang et al. (2016a), models which overestimate the Arctic sea-ice thickness, as does LIM2, have a too low September trend, while LIM3, which has a thinner ice, produces a realistic September trend.

20 In the SH, the LIM3 sea-ice edge is generally well located in the austral summer and the geographical distribution is correctly represented (Figure 1d, e). LIM3 sea ice is mostly confined to the western Weddell Sea, the southern Bellingshausen and Amundsen Seas and the southeast Ross Sea. Some differences with satellite observations are present. Notably, LIM3 underestimates the narrow fringe of sea ice around the East Antarctic coast and its sea ice also disappears excessively in the western Weddell Sea, where the model has a lower sea-ice concentration than observed, also indicating that its sea ice is too

25 thin regionally. The LIM2 sea-ice concentration is everywhere larger than the LIM3 one and the observed one across most of the Southern Ocean, with the largest differences in the Ross Sea and the eastern Weddell Sea (Figure 1f).

Both LIM models have a seasonal cycle of sea-ice extent with too large amplitudes (Figure 2c). Periods of sea-ice growth are shorter, and sea-ice growth/melt rates are faster than observed. In LIM3, the monthly minimum sea-ice extent in February is less than the observed, while the maximum sea-ice extent in September is overestimated with a seasonal amplitude of 19.2×10^6

30 km^2 (observed 16.0×10^6 km^2). The LIM2 minimum extent appears to be in better agreement with the NSIDC data, but the ice growth is even faster than in LIM3, and therefore clearly unrealistic. As a result, the LIM2 seasonal cycle amplitude is 19.9×10^6 km^2.

The time series of annual mean sea-ice extent of LIM3 is rather well reproduced and closely follows observations (Figure 2d), but the sea-ice summer retreat is systematically too strong and summer extent too low. The LIM3 low summer sea-ice

35 extent can be explained by the ice-albedo feedback, which is governed by the fast melting of thin ice enabling an effective

penetration of solar energy into the upper ocean. This occurs particularly in the marginal sea-ice zone, where the sea-ice concentration is low and ice thin. The effective ice-albedo feedback also promotes a higher bottom melt leading to thinner ice. Due to its multi-category sea-ice thickness distribution, these processes significantly reduce the LIM3 sea-ice concentration in summer compared to LIM2.

5   In the SH in September, both LIM models present statistically significantly increasing sea-ice extent anomaly trends, consistent with observations. However, these modelled September trends are larger than the observed trend. The increase of the Antarctic sea-ice extent has been explained by a range of mechanisms. Many studies attribute the increase of sea-ice extent to changes in the atmospheric dynamics, mainly by the increasing trend of the Southern Annular Mode, which in turn has strengthened westerly winds around the Antarctic continent and deepened the Amundsen Sea Low. Stronger westerlies ef-

10 fectively spread sea ice to north and a deeper Amundsen Sea Low increases the sea-ice production in the Ross Sea (see for example, Lefebvre and Goosse, 2008; Holland and Kwok, 2012; Massonnet et al., 2013; Turner et al., 2015). Another potential, simultaneously affecting mechanism increasing the sea-ice extent is the freshening of the Southern Ocean surface, which stabilises the surface layer, reduces the oceanic heat from below and therefore the associated ice melt (see for example Hellmer, 2004; Bintanja et al., 2013). Our model configurations do not implement the inter-annually increasing freshwater forcing, but

15 despite that are able to reproduce the increase of winter Antarctic sea-ice extent. This implies that changes in windiness are likely to be a major mechanism driving the SH sea-ice extent increase. Notably, the LIM modelled trends are larger than the observed ones, which may indicate a too sensitive ice drift response to increasing windiness, a too fast moving model sea ice and a too far northern winter sea-ice edge, as also supported by earlier studies (Uotila et al., 2014; Lecomte et al., 2016).

3.2   Sea-ice volume

20 In the NH, the monthly mean LIM3 sea-ice volume, which is the domain integral of the sea-ice thickness multiplied by sea-ice area per grid cell, varies from the minimum of 2.9×10^3 km^3 in September to the maximum of 8.8×10^3 km^3 in April. Both values are approximately 20% larger than the PIOMAS output. LIM2 and LIM3 maxima agree, but their September minima do not, with the LIM2 ice volume minimum being almost 30% larger. The evolution of the annual mean sea-ice volume in the 1958–2012 period is comparable in both models and, as in the case of sea-ice extent, shows significant inter-annual

25 variations. As with the sea-ice extent, NEMO-LIM simulations capture the large decrease of sea-ice volume during their last decade, 2003–2012, at a rate of -3.4 (-6.6)$\times 10^3$ km^3/decade in LIM3 (LIM2), while the PIOMAS rate is smaller, -2.0$\times 10^3$ km^3/decade.

In the SH, the LIM models' monthly mean sea-ice volume reaches its maximum in October and then decreases to 1,600 km^3 in February. The GIOMAS monthly mean sea-ice volume maximum occurs already in September from which it decreases to

30 2,800 km^3 in February. In general, the GIOMAS monthly mean sea-ice volume is higher than the LIM ones, with a distinctly different seasonal evolution. When comparing the LIM SH sea-ice volumes with GIOMAS, one should remember that the LIM3 SH sea-ice extent is smaller and closer to the observed than the one of LIM2. Hence, the LIM3 mean ice thickness, which is the ratio between sea-ice volume and extent, is more realistic than the LIM2 mean ice thickness, because their sea-ice

volumes are rather similar. LIM3 sea-ice volume growth rate is ∼30% less than the GIOMAS one, but ∼10% higher than the LIM2 one. In both LIM models, the periods of ice growth are typically longer and periods of melt shorter than in GIOMAS.

As with the sea-ice extent in the SH, the annual mean LIM3 sea-ice volume has a significant positive trend of 1.7×10^3 km^3/decade over the past decade 2003–2012. In contrast, the GIOMAS sea-ice volume trend for the same period is significantly

5 negative, -1.4×10^3 km^3/decade, while LIM2 has no significant trend. This indicates that, unlike in the NH, three models disagree in terms of the evolution of Antarctic sea-ice volume, at least for this particular time period.

There are important differences between PIOMAS and NEMO-LIM, explaining the systematic deviation of their sea-ice volume from each other. First, PIOMAS uses NCEP based atmospheric forcing compared to the DFS one used in the NEMO-LIM simulations. Second, PIOMAS assimilates sea-ice concentration and SST data, while the NEMO-LIM simulations do not.

10 Finally, PIOMAS ocean and sea-ice models and the computational grid are different from NEMO-LIM ORCA1 configurations along with numerous physical parameterisations implemented in the models.

In general, close similarities between the LIM2 and LIM3 sea-ice distributions in the SH emphasise the importance of the ocean model dictating the evolution of sea ice, while the level of sophistication of sea-ice model has a smaller importance. This is, at least partly, due to the divergent large-scale sea-ice motion where sea-ice deformation remains small (Uotila et

15 al., 2000). Therefore, different sea-ice deformation parameterisations in LIM2 and LIM3 have a lesser significance as in the relatively shallow Arctic Ocean. Another difference between LIM2 and LIM3 is related to the sea-ice thickness distribution parameterisation, which again has a smaller importance in the Southern Ocean than in the Arctic due to a smaller role of the ice-albedo feedback and the lack of surface melt ponds on the Antarctic sea ice compared to oceanic effects.

3.3 Sea-ice drift

20 The simulated March and September mean (2003–2012) sea-ice velocities are shown in Figure 3, together with the OSI SAF sea-ice drift product (Lavergne et al., 2010). Both LIM models realistically represent observed large-scale ice drift patterns, which are a direct response to the atmospheric circulation.

In the NH, the LIM3 mean drift pattern in March consists of an offshore motion over Siberian shelves (4–6 cm/s), the anti-cyclonic gyre in the Beaufort Sea (2–4 cm/s), the transpolar drift (4–6 cm/s) from the coast of Eastern Siberia to Fram Strait

25 (Figure 3c). The ice drift through Fram Strait and in the East Greenland Current is particularly strong (16–20 cm/s), as well as the southward drift (14–16 cm/s) through Davis Strait. The Arctic sea-ice velocities in both LIM models are generally higher compared to satellite estimates, and the location of the centre of the Beaufort Gyre is displaced westward, toward the Chukchi Sea (Figure 3a, c and e). A similar positive sea-ice velocity bias was reported by (Chevallier et al., 2015) who analysed 14 ocean-ice reanalysis products. This discrepancy might be a result of a too high air-sea momentum flux driving the ice too fast

30 and, on the shelf regions, due to the lack of a fast-ice parameterisation. On the other hand, the OSI SAF satellite derived sea-ice velocities may have high uncertainties over those regions of highly concentrated and slowly moving ice.

The two LIM models perform somewhat differently in terms of sea-ice speed, LIM2 sea ice being generally faster, in particular in the Beaufort Gyre, but then again weaker in the Nansen Basin (Figure 3e). The 10-year mean Arctic sea-ice velocity in March is 4.6 (4.8) cm/s for LIM3 (LIM2). Time series of area export through Fram Strait present similar variability

in both LIM simulations. During the last simulated decade, the annual mean area fluxes through Fram Strait correspond to more than 10% of the winter ice covered area, being 0.86 (0.89) million km^2 in LIM3 (LIM2), both being comparable to estimates based on SAR data (Smedsrud et al., 2011).

In the SH, the LIM models feature similar and realistic looking distribution of the September ice drift (Figure 3). They

5   show realistic patterns of the Weddell and Ross Gyres, the westward coastal and eastward offshore circumpolar currents. The observed OSI SAF drift generally compares well with the modelled ones in terms of their large-scale velocity field patters although the modelled speeds appear faster than observed, particularly along the ice edge. That suggests that LIM models simulate the Antarctic sea-ice drift reasonably well albeit somewhat too fast which seems to be a consistent ocean-ice model bias (Uotila et al., 2014).

10   As in the Arctic, the two LIM models have similar sea-ice velocity magnitude within the central ice pack, but larger differences appear close to the ice edge, where the LIM3 ice drift is ∼2 cm/s faster than LIM2, and in the coastal areas, where LIM2 speed is ∼2 cm/s faster than LIM3 (Figure 3f). Close to the ice edge, LIM3 has a smaller ice extent and a lower ice concentration at regions. There the LIM3 ice motion is closer to the free drift and therefore faster that LIM2 ice motion. In the coastal areas, differences in ocean currents and ice deformation parameterisations are likely causes for the velocity differences

15   between the LIM models. The horizontal, perpendicular-to-coast salinity gradient is stronger in LIM2 than in LIM3 in a way that LIM2 coastal surface waters are fresher, while off the coast LIM2 surface waters are saltier than in LIM3. This difference in the salinity gradient modifies the density gradient, coastal geostrophic currents and ice drift along the coast.

3.4   Sea-ice salinity

One important new feature in LIM3 is the prognostic sea-ice salinity compared to the constant 4 ppm sea-ice salinity in LIM2

20   (Vancoppenolle et al., 2009a). LIM3 explicitly includes the salt water entrapment and drainage in sea ice, where it also impacts on the ice thermodynamic variables such as the specific heat, conductivity and enthalpy. Furthermore, when snow-ice is formed by flooding and freezing of a relatively thick snow layer on top of ice, the LIM3 snow-ice becomes saline in contrast to the LIM2 fresh snow-ice. Vancoppenolle et al. (2009b) found that these improvements impacted on the LIM sea-ice volume, and that the LIM3 sea ice compared better with observations than the LIM2 sea ice.

25   This improved realism is existing in our simulations, as shown in previous sections describing the LIM sea-ice extent and volume. It is likely that to some extent the more realistic LIM3 sea ice is due to the advanced salinity dependent halo-thermodynamics and a more realistic seasonal cycle of sea-ice salinity, and associated upper ocean freshwater fluxes. In winter, newly formed LIM3 sea ice preserves a higher salinity than in LIM2 (Figure 4). In contrast, in summer, the remaining LIM3 sea ice has a 2–4 ppm lower salinity than LIM2 in the Arctic. However, during the Antarctic summer, the LIM3 sea-ice salinity

30   stays relatively high, except at the ice edge. This is due to the fact that even in summer air temperature remains at freezing over the coastal Antarctic seas. As in Vancoppenolle et al. (2009b), our simulations confirm that the LIM3 prognostic sea-ice salinity behaves realistically and compares well with the available observations.

4 Sensitivity simulations

Based on rather descriptive analysis of differences between the LIM models, presented in the previous section, we have gained a relatively comprehensive understanding of how their global sea-ice distributions compare. In this section, we address what makes LIM3 sea ice different from LIM2 sea ice. Model grid and atmospheric forcing are identical; sea-ice differences can only

5   arise from differences in sea-ice model physics parameterisations and these differences can be further amplified by ocean-ice feedback processes. To find out which parameterisations are of importance in producing LIM model differences, we performed and analysed some additional simulations.

4.1 NEMO-LIM3 single-category simulation

LIM3 differs from LIM2 in two important aspects: LIM3 has a multi-category sub-grid-scale sea- ice thickness distribution

10   and multilayer halo-thermodynamics scheme with prognostic non-constant sea-ice salinity profile. We tested the effect of these parameterisations by carrying out a LIM3 simulation with a single-category sea-ice thickness distribution having a virtual ice thickness distribution and a constant 4 ppm sea-ice salinity. Importantly, by setting the LIM3 sea-ice salinity constant, along with its two vertical ice layers and one snow layer, its thermodynamics scheme becomes similar to the LIM2 one. However, the initialisation procedure of LIM3 is different from the one used in LIM2, as explained in Section 2.3. We denote the LIM3

15   single-category simulation as LIM3MC.

In terms of NH sea-ice extent, LIM3MC is located between LIM3 and LIM2, and in the SH its annual-mean sea-ice extent follows closely to the one of LIM2 (Figure 2b and d). However, the monthly sea-ice extent climatology of LIM3MC is distinctly closer to LIM3 and does not have the distorted shape of LIM2 monthly sea-ice extent climatology (Figure 2a and c). Furthermore, the summer minimum and winter maximum of LIM3MC sea-ice extents differ significantly from LIM2 ones.

20   This result suggests that the use of the single-category and constant salinity parameterisations brings LIM3 sea ice closer to LIM2 output, as expected, but significant differences remain.

The LIM3MC sea-ice volume relative to two other LIM simulations is more different in the SH than in the NH. In the Southern Hemisphere, the LIM3MC sea-ice volume immediately diverts from LIM2 and LIM3, although its annual mean sea-ice extent remains rather close to LIM2 with a seasonal variability closer to the LIM3 one. It is possible that strong ocean-ice

25   feedback processes in LIM3MC affect the melting and freezing rates during its first simulation year, and associated fluxes of salt and freshwater. This in turn modifies the upper ocean stratification and oceanic heat, which result in further differences in LIM3MC sea-ice volume that adjusts above the LIM2 level. The 20 cm thicker LIM3MC initial snow might have contributed to the differences in sea-ice thickness between LIM2 and LIM3MC by reducing the spring melt at the end of the first simulation year resulting in a relatively high sea-ice volume minimum in summer that persists through the simulation. After this, the high

30   LIM3MC sea-ice volume seems to be in a balance with the upper ocean adjusted during the first years of the simulation.

In addition to sea-ice thermodynamics, the sea-ice salinity scheme modifies the ocean-ice salt and freshwater exchange, and upper ocean heat fluxes, which influence the evolution of sea ice. Compared to LIM2, the LIM3 multi-category sea-ice is saltier in winter due to its prognostic sea-ice salinity (Figure 4). This implies a smaller ocean-to-ice salt flux during freezing

and a more stably stratified ocean surface layer, particularly in the Southern Ocean and in the Barents Sea where LIM3–LIM2 winter salinity differences seem particularly large (Figure 4). If the LIM3 prognostic salinity was of primary importance, we would expect a higher sea-ice volume in the LIM3 prognostic sea-ice salinity simulation than in the LIM3MC constant sea-ice salinity simulation due to smaller salt rejection rates and associated ocean convection in the Southern Ocean. As this is not the case, the importance of the sea-ice salinity scheme, in modifying the sea-ice evolution by affecting upper ocean heat fluxes, appears to be a secondary one compared to the effects of sea-ice salinity scheme on sea-ice thermodynamics and especially to the effects of sub-grid-scale ice thickness parameterisation.

4.2 Effects of freshwater adjustments

Following a common practise when carrying out forced ocean-ice simulations, we applied a fresh water budget adjustment and SSS restoring in our simulations. The freshwater budget, evaporation minus precipitation minus river runoff, was adjusted from the previous year's annual mean budget to zero at the beginning of each simulation year.Additionally, we added a SSS dependent flux correction term on freshwater fluxes. This flux correction term practically damps the model top-level salinity towards the PHC3 top level salinity PHC3 everywhere, also under sea ice, in LIM2, LIM3 and LIM3MC simulations. These treatments prevent an unrealistic drift of the sea surface height due to errors in the prescribed freshwater budget components.

In addition to the common practise, we completed two otherwise identical integrations, one for LIM2 and one for LIM3, where we turned off the two freshwater adjustment mechanisms to see what kind of effect they have on our results. As expected, the ocean salinity drift became significant in the non-adjusted simulations, being strongest in the top layer, increasing its salinity by 0.4 psu in 54 years. This salinity change resulted in a global sea-level decrease of 8 m and also modified the ocean density structure. Related to this, a shallower mixed layer in the northern North Atlantic, a slightly weaker (1-2 Sv) Atlantic Meridional Overturning Circulation (AMOC), and a somewhat larger temperature drift were detected from the non-adjusted stimulations.

Perhaps interestingly and in contrast to the North Atlantic, the Southern Ocean mixed layers were deeper without freshwater adjustments. Importantly, for the scope of this study, the effects of freshwater adjustments on sea-ice evolution were minuscule. LIM models produced almost identical sea ice, and therefore essentially identical ocean-ice differences, independent of whether the freshwater adjustments were turned on or off. This result implies that in coupled atmosphere-ocean NEMO-LIM configurations, where the freshwater adjustments must be turned off, the ocean-ice coupling is unlikely to generate issues. In other words, if problems appear, they are related to the coupling and flux exchanges between the oceanic and atmospheric components.

5 Ocean hydrography and circulation

5.1 Arctic surface salinity

We now move on to explore differences in ocean properties between the two LIM versions. Figure 5 shows LIM3 Arctic SSS and sea-surface temperature (SST) averaged over the last decade of the simulation, 2003–2012, and its departures from PHC3,

WOA13 and LIM2. LIM3 differences from PHC3 and WOA13 are much larger than its differences from LIM2, highlighting the fact that the LIM version has a secondary impact on the Northern Hemispheric ocean properties.

LIM3 surface salinity distribution realistically reflects the fact that the Arctic Ocean has a low salinity surface layer in contrast to the much saltier surface layer of the North Atlantic (Figure 5a). Compared to PHC3 and WOA13, both NEMO-LIM

5 versions are too fresh in the North Atlantic, Labrador Sea and Nordic Seas, although the LIM3 Labrador Sea surface is slightly saltier than that of LIM2 (Figure 5b–d). In the Greenland Sea, the LIM3 fresher surface compared to LIM2 is related to the melted freshwater from excessive sea ice. In some parts of the Eurasian Basin, LIM3 is saltier than PHC3 partly associated with its negative sea-ice concentration bias and the lack of fresh melt water (Figure 5b). Compared to WOA13, LIM3 SSS is much higher due to the SSS restoring toward PHC3, which indicates observational disagreements in terms of Arctic SSS and

10 that the PHC3 SSS is higher than WOA13 SSS. As PHC3 was carefully constructed for the Arctic, it is plausible that its SSS climatology is closer to the truth. LIM ocean salinity biases mainly arise from the NEMO ocean model configuration, and the applied boundary conditions, such as the atmospheric forcing, river runoff and freshwater adjustments.

LIM3 has a fresher surface than LIM2 in many areas on the Siberian shelf, Barents Sea and Greenland Sea, associated with the smaller ice-ocean salt flux, thicker ice in winter and larger melt rates during spring. By contrast, in LIM2, fresher ice and

15 reduced spring melt result in an increased ice-to-ocean salt flux and therefore higher SSS in those regions. However, along the East Greenland coast and in the Labrador Sea, thicker sea ice is associated with higher melt rates and result in a fresher surface. These differences in surface salinity, associated with sea-ice differences, have potential implications for the strength of AMOC, as discussed below. Hence, although mutual hydrographic differences between the LIM simulations are small compared to their observational biases, they may potentially have an impact on the convective processes in the North Atlantic.

20 **5.2 Arctic surface temperature**

As with SSS, SST differences between the LIM models in the Arctic are small compared to their differences from PHC3 and WOA13 (Figure 5f–h). The LIM models have a distinct cold bias in the North Atlantic and in the Greenland Sea. In the Norwegian and Barents Seas, LIM3 surface is warmer than PHC3, while its difference to WOA13 is relatively small. The WOA13 climatology represents years 2005–2012 and better matches the NEMO-LIM analysis period of 2003–2012 than

25 PHC3, which contains observations before 2005. As PHC3 SST is colder than WOA13 and LIM3 SSTs in the Norwegian and Barents Seas, it is evident that these differences are related to the recent warming of these regions.

Related to the larger LIM2 sea-ice extent, LIM2 SST is colder than LIM3 SST across most of the Arctic Ocean, along the East Greenland coast, in Baffin Bay and in the Labrador Sea. In contrast, SST in the Norwegian Sea and Barents Sea is lower in LIM3 than LIM2, associated with a lower salinity. In these regions, saltier LIM2 surface waters release less heat to the

30 atmosphere before reaching the critical density and sinking down, which explains the warmer LIM2 SST. Additionally, these regions have a deeper LIM2 mixed layer, as we will soon show. These SSS, SST and MLD differences signify a more effective upper ocean convection in the LIM2 simulation.

5.3 Southern Ocean surface salinity

In the SH, LIM and PHC3/WOA13 SSS differences are smaller than in the NH (Figure 6b, c). In the regions covered by sea ice, the LIM3 ocean surface is fresher than PHC3, except in some areas along the East Antarctic coast. These coastal differences are smaller between LIM3 and WOA13 than between PHC3 (Figure 6b, c), which could be related to a larger number of better

5 quality coastal Antarctic observations included in WOA13 and the fact that the simulation analysis period temporally better matches with WOA13 than PHC3. LIM3 SSS differences with LIM2 form to some extent a similar spatial pattern than its differences with PHC3, although LIM3–LIM2 differences have smaller magnitudes (Figure 6d). Now, LIM2 Antarctic sea ice is more extensive, but thinner than LIM3 sea ice, on the average. Hence, off the Antarctic coast where the ice melts, less fresh water is released per area in LIM2 than in LIM3 resulting in a higher LIM2 SSS. Close to the Antarctic coast the LIM2 ocean

10 surface is fresher than the LIM3 ocean surface. This is likely to be be due to the smaller winter ice formation rates in LIM2, associated smaller salt flux from ice to ocean.

Processes related to the LIM3 and PHC3/WOA13 SSS discrepancies in the Southern Ocean are likely to be associated with the other freshwater sources rather than the sea ice related fresh water exchange. Again, this is because the LIM and PHC3/WOA13 differences are of larger magnitudes than the differences between two LIM models. Most important external

15 freshwater sources in the Southern Ocean are precipitation and melt water fluxes from the Antarctic continental ice sheet, and both of these sources are known to have large uncertainties. Given these observational freshwater and SSS uncertainties, we can expect significant differences between NEMO-LIM and PHC3/WOA13 ocean surface characteristics. However, as the NEMO-LIM simulations applied the SSS restoring, LIM and PHC3 sea-surface salinities did not evolve very far apart compared to the simulations where the freshwater was not adjusted (not shown).

20 ### 5.4 Southern Ocean surface temperature

LIM3 surface is colder than PHC3 and WOA13 around the East Antarctica (Figure 6f, g). As this difference is associated with fresher surface and lower than observed ice concentration, it is likely that the more stable LIM3 surface stratification decreases the upward oceanic heat flux and increases the surface heat loss to the atmosphere due to larger open water areas. Consistent with this explanation, the higher LIM2 sea-ice concentration and SSS seem to result in a higher SST than the one of LIM3

25 around the East Antarctic (Figure 6h).

5.5 Arctic intermediate water (AIW)

In the Arctic Ocean, approximately at 250 m depth, lies the relatively warm AIW layer that originates from the Atlantic Ocean (Figures 7 and 8). AIW is below the halocline and therefore saltier than waters above it (Figures 7h and 8b). The NEMO-LIM models simulate too fresh and cold waters at 250 m in the Arctic Ocean (Figure 7b-c, f-g). During the first decade of NEMO-

30 LIM simulations, their AIW layers cool and possibly due to too vigorous mixing loose heat to the water masses above resulting in weaker and broader thermoclines than PHC3 and WOA13 (Figure 8a).

LIM3 AIW remains warmer than LIM2 (Figure 8a), which indicates a somewhat larger Atlantic warm water inflow into the Arctic Ocean and might be associated to a smaller meridional overturning circulation in the North Atlantic in LIM3. Unlike in the Arctic Ocean, in the Nordic Seas and Barents Sea PHC3 and WOA13 are colder than LIM3 at 250 m (Figure 7f, g). This indicates that not enough oceanic heat enters the Arctic Ocean in the LIM simulations possibly due to their coarse model grid

5   that does not adequately resolve the basin topography and eddy heat transport. The lack of warm Atlantic water inflow to the Arctic and associated biases are consistent with the ones founded in the multi-model study by Wang et al. (2016b).

5.6   Temperature and salinity differences outside the Polar Regions

Outside the polar regions, small temperature and salinity differences emerge as the LIM simulations proceed. For example, LIM3 has a saltier Atlantic Ocean than LIM2 at the layer from the surface to 1000 m depth. LIM salinity differences vary in

10   time with maximum values up to 0.05 psu, while their Atlantic basin averaged salinities are approximately 35.35 psu. On the basin scale, salinity differences between the two LIM simulations above 1000 m depth become notable rather soon, during the first decade of simulations. In other basins, salinity and temperature differences above 1000 m depth and outside the polar regions remain much smaller. However, in the Atlantic Ocean in the layer deeper than 1000 m, LIM2 starts to evolve into a saltier and warmer state than LIM3 from the late 1970s onward. There basin-wide mean salinity differences amount up to

15   0.001 psu by the end of simulations. At the same time, in the layer deeper than 1000 m of the Pacific Ocean, LIM3 becomes on the average saltier and colder than LIM2. Changes in these deep water characteristics originate from the surface perturbations, which are slowly transported deeper by the meridional overturning circulation and deep water formation. The key regions where atmosphere-ocean conditions permit the deep water formation and consequently drive the meridional overturning circulation are located in the northern North Atlantic and coastal Antarctica. These are also the regions where the sea-ice cover between

20   the two LIM simulations vary and thus modify the atmosphere-ocean energy exchange, which then affects the deep water formation and the World Ocean meridional overturning circulation.

5.7   Mixed layer depth (MLD)

Oceanic convection, vertical heat transport and deep water formation are intimately related to the MLD. We keep in mind that the observational MLD uncertainties are particularly large in ice covered oceans, because of sparse observations, and therefore

25   limit our comparisons to the North Atlantic and the Southern Ocean. In Figure 9, the mean winter MLD is presented for LIM3 along with its difference from the observed climatology of de Boyer Montégut et al. (2004), and for the LIM3–LIM2 difference. Clearly, the regions of deep MLD are located off the sea-ice edge.

In the Greenland Sea, the observed MLD is deeper than the LIM3 MLD (Figure 9b). This could be due to excessive winter LIM3 sea ice in the East Greenland Current resulting in a shallower LIM3 mixed layer. The presence of sea ice diminishes

30   the heat loss and reduces the MLD. Furthermore, the region south of Greenland in the North Atlantic, characterised by cold and fresh LIM3 biases, also has a shallower than observed mixed layer. This is to be expected due to the more stable LIM3 surface stratification compared to PHC3. In the Norwegian Sea and the Barents Sea, the LIM3 MLD is much larger than the observational MLD indicating stronger oceanic convection (Figure 9b). This is at least partly due to cold, non-responsive and

prescribed winter atmosphere acting as an infinitive heat sink to the relatively warm ocean surface layer and associated with relatively cold LIM3 SSTs (section 5.2).

In the Southern Ocean, the observed mixed layer is much shallower than the LIM3 mixed layer outside the regions covered by ice, particularly in the Pacific sector (Figure 9e). This pattern, to some extent, resembles the MLD difference pattern in the
5 Norwegian Sea and the Barents Sea. In the Southern Ocean, as in the North Atlantic, the very deep LIM3 MLD is a likely response to the prescribed atmospheric forcing and possibly to erroneous precipitation and freshwater fluxes originating from the Antarctic ice sheet.

Although the LIM2 MLD generally appears to be relatively close to the LIM3 one in the Arctic, it is approximately 10-20% deeper in the Nordic Seas and the Barents Sea (Figure 9c). These are also regions where the LIM2 SSS is higher than the LIM3
10 one, and where denser LIM2 surface entrain deeper resulting in a deeper mixed layer than in LIM3, which, as we will show, is associated with a stronger AMOC in LIM2. In the Southern Ocean, LIM MLD differences are quite small, with most distinct ones visible in the Antarctic coastal areas (Figure 9f). As these are the regions of the Antarctic Bottom Water formation, MLD differences indicate differences in the locations and rates of the deep water formation between the two LIM simulations. This variability in the deep water formation changes the deep water properties, which is manifested as slowly emerging differences
15 in abyssal temperature and salinity, decades after the beginning of simulations, as discussed earlier in section 5.6.

5.8 Atlantic Meridional Overturning Circulation (AMOC)

An important characteristic of a global ocean model is the strength and extent of its AMOC. Danabasoglu et al. (2014) assessed the mean AMOC of eighteen ocean-ice models forced by prescribed atmospheric forcing from 1948–2007 and run five repetitive forcing cycles, restarted from the state at the end of the previous cycle. Many of these fifteen ocean models were
20 also used as the ocean-ice components of CMIP5 climate models. Here, results of Danabasoglu et al. (2014) provide a useful indicative benchmark for our NEMO-LIM simulations, although one needs to keep in mind differences between CORE-II and our experiment setup, which are likely to affect AMOC. In Figure 10, the time evolution of LIM3 AMOC looks rather similar to some ocean-ice models assessed by Danabasoglu et al. (2014) during their first simulation cycle (compare Danabasoglu et al. (2014) Figure 1, middle panel and our Figure 10a). As LIM3, these models initially have an AMOC of 16-17 Sv which
25 gradually, during the first three decades, decreases down to 8-12 Sv. These models, labelled as NOCS, CERFACS and CMCC in Danabasoglu et al. (2014), are based on earlier versions of NEMO than NEMO3.6, but importantly share the identical ORCA1 horizontal grid with us. The NOCS model has 75 vertical levels, as our NEMO-LIM configurations, while CERFACS and CMCC have a smaller number of vertical levels.

In addition to AMOC temporal evolution, our mean AMOC transport patterns in depth-latitude space well resemble the
30 NEMO ORCA1 ones of Danabasoglu et al. (2014). This can be seen by comparing our Figure 10c with their Figure 3. In particular, NOCS and CMCC mean patterns resemble our NEMO-LIM3 pattern with high northward transport regions at 1000 m, a surface maximum at 10-20°N, and a rather strong southward transport approximately at 4000-5000 m (not shown). These qualitative inspections with Danabasoglu et al. (2014) indicate that our NEMO- LIM simulations produce a comparable AMOC to earlier NEMO configurations with comparable horizontal and vertical resolutions.

Deviations between the LIM2 and LIM3 simulations in terms of their AMOC are minor. There are, however subtle differences, as seen from Figure 10a, where the LIM2 annual maximum AMOC within the 50-53°N band is up to 0.4 Sv stronger than the LIM3 AMOC within the same latitude band. The stronger LIM2 AMOC is likely to be driven by stronger deep convection in the Nordic Seas, apparent as a deeper MLD. As explained earlier, differences in MLD are related to differences in

5 ocean surface stratification caused by deviations in sea-ice characteristics between the two LIM simulations.

5.9 Other oceanic transports

In addition to AMOC, LIM simulations show slightly varying volume transports in other major transects, such as the Drake Passage (Figure 10b). There, LIM2 volume transports became approximately 5 Sv larger than in LIM3. These are relatively small deviations, given the fact that total volume transports in the Drake Passage are around 160 Sv. However, it is possible

10 that these deviations further increase during long, multi-centennial simulations, as demonstrated by Danabasoglu et al. (2014) with respect of AMOC.

6 Conclusions

A set of hindcast simulations (1958–2012) were performed with the newest NEMO3.6 model in the global ORCA1 grid forced by the DFS5.2 atmospheric data. The primary objective was to diagnose the sensitivity of the NEMO-LIM ocean-ice system

15 to the representation of physics in the sea-ice model. Results of such analysis have not been published for the newest NEMO in the nominal 1° latitudinal resolution, which is used as the ocean-ice component in many climate models participating in the CMIP6 project. We focussed on two simulations that differ only in their sea-ice component: the widely-used LIM2 and its successor, LIM version 3.6. The main differences between the two sea-ice models lie in their parameterisation of sub-grid-scale sea-ice thickness distribution, ice deformation, thermodynamic processes, and sea-ice salinity.

20 To assess the performance of two LIM versions, we briefly compared their climatological sea-ice distributions mutually and with observational estimates. In terms of global sea ice, LIM3 compares clearly better with available observations, while LIM2 deviates more, producing too much ice in the Arctic, for example. The better representation of the ice-albedo feedback makes LIM3 more capable in simulating the September minimum of extent than LIM2, including the 2007 extremely low Arctic value. These sea-ice findings are consisted with the ones of Vancoppenolle et al. (2009b); Massonnet et al. (2011); Vancoppenolle et

25 al. (2015); Rousset et al. (2015).

It is worth noting that no specific NEMO-LIM tuning was done for our experiments. It is likely that after some adjustments, such as controlled changes in the sea-ice albedo or ice strength, the NEMO-LIM3 sea-ice performance will to some extent increase (Uotila et al., 2012). It is also worth noting that NEMO-LIM3 has been developed further and, for example, a new sea-ice albedo scheme was implemented in April 2016. Our preliminary tests on this new scheme demonstrate the robustness

30 of LIM3, as its sea-ice distribution appears almost insensitive to changes in summer albedo. This robustness also signifies that the results of this study remain valid even after the implementation of the new albedo scheme. The differences between

NEMO-LIM2 and NEMO-LIM3 seem robust, as they do not significantly change even after switching the NEMO ocean surface freshwater adjustments off.

Our model evaluation focussed on the upper ocean properties and to some extent oceanic transports across major transects of the World Ocean, such as the Drake Passage, along with its meridional overturning circulation. This has not been systematically
5   done before for NEMO3.6. In general, ocean hydrographic differences, such as temperature and salinity, between the two LIM versions are confined to the upper ocean and near the sea-ice zone. In terms of large-scale ocean circulation, differences between the two LIM versions remained small, but kept increasing over the decades, also in the extra-polar regions.

As a further sensitivity experiment, we repeated the NEMO-LIM3 hindcast simulation after setting its sea-ice distribution to the single-category mode. At large and as expected, this single-category configuration resulted in a shift of LIM3 sea-ice
10   distribution towards the LIM2 one, but encouragingly the LIM3 single-category sea ice remained clearly more realistic than the LIM2 one. This result indicates that one option for modellers who are considering in upgrading from LIM2 to LIM3, is to start using the single-category LIM3 as an intermediate step. Based on these findings, we conclude that NEMO3.6 is ready as a stand-alone ocean-ice model and as a component of coupled atmosphere-ocean models.

7   Code and data availability

15   The NEMO version 3.6 version incorporates LIM2 and LIM3.6 sea-ice models, and can be downloaded from the NEMO web site (http://www.nemo-ocean.eu/) at this address: http://forge.ipsl.jussieu.fr/nemo/svn/branches/2015/nemo_v3_6_STABLE. The model input data can be obtained following the references described in section 2.5. The output of model simulations and the computer scripts used to produce the results presented in the paper, including the figures, are available from the corresponding author upon request.

20   *Acknowledgements.* We acknowledge the creators of low resolution sea-ice drift product of the EUMETSAT Ocean and Sea Ice Satellite Application Facility (OSI SAF, www.osi-saf.org). We thank Dr Laurent Brodeau for providing us the very useful Barakuda software package to diagnose NEMO simulations. The work of Lensu and Uotila was supported by the Academy of Finland (contracts 264358 and 283034).

References

Amante, C. and B.W. Eakins (2009), ETOPO1 1 Arc-Minute Global Relief Model: Procedures, Data Sources and Analysis. NOAA Technical Memorandum NESDIS NGDC-24. National Geophysical Data Center, NOAA.

Blanke, B. and P. Delecluse (1993), Low frequency variability of the tropical Atlantic Ocean simulated by a general circulation model with mixed layer physics. J. Phys. Oceanogr., 23, 1363– 1388.

Beckmann, A. and D. B. Haidvogel (1993), Numerical simulation of flow around a tall isolated seamount. Part I - problem formulation and model accuracy. J. Phys. Oceanogr., 23 (8), 1736–1753.

Bintanja, R., van Oldenborgh, G. J., Drijfhout, S. S., Wouters, B. and Katsman, C. A. (2013), Important role for ocean warming and increased ice-shelf melt in Antarctic sea-ice expansion. Nature Geoscience, 6(5), 376-379.

Bitz, C.M., Lipscomb, W.H. (1999), An energy-conserving thermodynamic model of sea ice, Journal of Geophysical Research 104, 15669–15677.

Bouillon, S., M.A. Morales Maqueda, V. Legat, and T. Fichefet (2009), An elastic-viscous-plastic sea ice model formulated on Arakawa B and C grids. Ocean Modelling, 27, 174-184.

Bouillon, S., T. Fichefet, V. Legat, and G. Madec (2013), The elastic-viscous-plastic method revisited, Ocean Model., doi:10.1016/j.ocemod.2013.05.013.

de Boyer Montégut, C., G. Madec, A. S. Fischer, A. Lazar, and D. Iudicone (2004), Mixed layer depth over the global ocean: an examination of profile data and a profile-based climatology, J. Geophys. Res., 109, C12003, doi:10.1029/2004JC002378.

Boyer, T.P., J. I. Antonov, O. K. Baranova, C. Coleman, H. E. Garcia, A. Grodsky, D. R. Johnson, R. A. Locarnini, A. V. Mishonov, T.D. O'Brien, C.R. Paver, J.R. Reagan, D. Seidov, I. V. Smolyar, and M. M. Zweng (2013), World Ocean Database 2013, NOAA Atlas NESDIS 72, S. Levitus, Ed., A. Mishonov, Technical Ed.; Silver Spring, MD, 209 pp., http://doi.org/10.7289/V5NZ85MT.

Brodeau, L., B. Barnier, A.-M. Treguier, T. Penduff, and S. Gulev (2010), An ERA40-based atmospheric forcing for global ocean circulation models, Ocean Model., 31(3-4), 88–104, doi:10.1016/j.ocemod.2009.10.005.

Campin, J. M., J. Marshall, and D. Ferreira (2008), Sea ice-ocean coupling using a rescaled vertical coordinate z*, Ocean Model., 24(1-2), 1–14, doi:10.1016/j.ocemod.2008.05.005.

Chevallier, M. et al. (2015), Uncertainties in the Arctic sea ice cover in state-of-the-art ocean reanalyses from the ORA-IP project, Clim. Dyn., Special Issue, (published online), doi:10.1007/s00382-016-2985-y.

Coon, M. D., Maykut, G. A., Pritchard, R. S., Rothrock, D. A., and Thordnike, A. S (1974), Modeling the pack ice as an elastic-plastic material, AIDJEX Bull., 24, 1–106.

Danabasoglu, G. et al. (2014), North Atlantic simulations in Coordinated Ocean-ice Reference Experiments phase II (CORE-II). Part I: Mean states, Ocean Model., 73, 76–107, doi:10.1016/j.ocemod.2013.10.005.

Danabasoglu, G. et al. (2016), North Atlantic simulations in Coordinated Ocean-ice Reference Experiments phase II (CORE-II). Part II: Inter-annual to decadal variability, Ocean Model., 97, 65– 90, doi:10.1016/j.ocemod.2015.11.007.

Dee, D. P. et al. (2011), The ERA-Interim reanalysis: configuration and performance of the data assimilation system, Quarterly Journal of the Royal Meteorological Society, 137(656), 553–597, doi:10.1002/qj.828.

Downes, S. M. et al. (2015), An assessment of Southern Ocean water masses and sea ice during 1988–2007 in a suite of inter-annual CORE-II simulations, Ocean Model., doi:10.1016/j.ocemod.2015.07.022.

Dussin, R., B. Barnier, and R. Brodeau. (2014), The making of DRAKKAR Forcing Set 5. DRAKKAR/MyOcean Report 05-10-14.

Farneti, R. et al. (2015), An assessment of Antarctic Circumpolar Current and Southern Ocean Meridional Overturning Circulation during 1958–2007 in a suite of interannual CORE-II simulations, Ocean Model., doi:10.1016/j.ocemod.2015.07.009.

Fetterer, F., K. Knowles, W. Meier, and M. Savoie (2002), updated daily. Sea Ice Index. Boulder, Colorado USA: National Snow and Ice Data Center. http://dx.doi.org/10.7265/N5QJ7F7W.

5   Fichefet, T., and M.A. Morales Maqueda (1997), Sensitivity of a global sea ice model to the treatment of ice thermodynamics and dynamics. Journal of Geophysical Research, 102, 12,609-12, 646.

Gaspar, P., Y. Gregoris, and J.-M. Lefevre (1990), A simple eddy kinetic energy model for simulations of the oceanic vertical mixing Tests at station papa and long-term upper ocean study site. J. Geophys. Res, 95 (C9).

Goosse, H (1997), Modeling the large-scale behavior of the coupled ocean-sea ice system. PhD thesis, Université Catholique de Louvain,
10   Louvain-la-Neuve, Belgium.

Goosse, H. and T. Fichefet: Importance of ice-ocean interactions for the global ocean circulation: A model study. J. Geophys. Res., 104, 23337–23355, 1999.

Griffies, S. M. (2004), Fundamentals of ocean climate models, Princeton University Press, 528 pp.

Griffies, S. M. et al. (2009), Coordinated Ocean-ice Reference Experiments (COREs), Ocean Model., 26(1-2), 1–46,
15   doi:10.1016/j.ocemod.2008.08.007.

Griffies, S. M. et al. (2014), An assessment of global and regional sea level for years 1993–2007 in a suite of interannual CORE-II simulations, Ocean Model., doi:10.1016/j.ocemod.2014.03.004.

Hellmer, H.H. (2004), Impact of Antarctic ice shelf basal melting on sea ice and deep ocean properties. Geophys. Res. Lett., 31, L10307, doi: 10.1029/2004GL019506.

20   Hibler III, W.D., (1979), A dynamic–thermodynamic sea ice model, Journal of Physical Oceanography, 9, 815–846.

Holland, P. R., and R. Kwok (2012), Wind-driven trends in Antarctic sea-ice drift, Nature Geoscience, 5(11), 1–4, doi:10.1038/ngeo1627.

Hunke, E. C., and J. Dukowicz (1997), An elastic-viscous-plastic model for sea ice dynamics, J. Phys. Oceanogr., 27, 1849–1867.

IOC, IHO and BODC, 2003. Centenary Edition of the GEBCO Digital Atlas, published on CD-ROM on behalf of the Intergovernmental Oceanographic Commission and the International Hydrographic Organization as part of the General Bathymetric Chart of the Oceans,
25   British Oceanographic Data Centre, Liverpool, U.K.

IOC, SCOR, and IAPSO, 2010: The international thermodynamic equation of seawater - 2010: Calculation and use of thermodynamic properties. Tech. rep., Intergovernmental Oceanographic Commission, http://www. teos-10.org/pubs/TEOS-10_Manual.pdf

Kjellsson, J., P. R. Holland, G. J. Marshall, P. Mathiot, Y. Aksenov, A. C. Coward, S. Bacon, A. P. Megann, and J. Ridley (2015), Model sensitivity of the Weddell and Ross seas, Antarctica, to vertical mixing and freshwater forcing, Ocean Model., 94, 141–152,
30   doi:10.1016/j.ocemod.2015.08.003.

Kwok, R., and D. A. Rothrock (2009), Decline in Arctic sea ice thickness from submarine and ICESat records: 1958–2008, Geophysical Research Letters, 36(15), doi:10.1029/2009GL039035.

Large W.G., and S.G. Yeager (2004), Diurnal to decadal global forcing for ocean and sea ice models: the data sets and flux climatologies. Technical Report NCAR/TN460+STR, CGD Division of the National Centre for Atmospheric Research (NCAR).

35   Large, W. G., and S. Yeager (2009), The global climatology of an interannually varying air–sea flux data set, Clim. Dyn., doi:10.1007/s00382-008-0441-3.

Lavergne, T., Eastwood, S., Teffah, Z., Schyberg, H. and L.-A. Breivik (2010), Sea ice motion from low resolution satellite sensors: an alternative method and its validation in the Arctic. J. Geophys. Res., 115, C10032, doi:10.1029/2009JC005958.

Lecomte, O., H. Goosse, T. Fichefet, P. R. Holland, P. Uotila, V. Zunz, and N. Kimura (2016), Impact of surface wind biases on the Antarctic sea ice concentration budget in climate models, Ocean Model., under review.

Lefebvre, W. and Goosse, H. (2008), Analysis of the projected regional sea-ice changes in the Southern Ocean during the twenty-first century, Clim. Dynam., 30, 59–76.

Madec, G., and the NEMO team (2015), NEMO ocean engine - version 3.6 stable. Note du Pôle de modélisation de l'Institut Pierre-Simon Laplace (IPSL), France, No 27 ISSN No 1288-1619.

Massonnet, F., T. Fichefet, H. Goosse, M. Vancoppenolle, P. Mathiot, and C. Konig Beatty (2011), On the influence of model physics on simulations of Arctic and Antarctic sea ice. The Cryosphere, 5, 687–699.

Massonnet, F., P. Mathiot, T. Fichefet, H. Goosse, C. König Beatty, M. Vancoppenolle, and T. Lavergne (2013), A model reconstruction of the Antarctic sea ice thickness and volume changes over 1980–2008 using data assimilation, Ocean Modelling, 64, 67–75, doi:10.1016/j.ocemod.2013.01.003.

Meier, W., F. Fetterer, M. Savoie, S. Mallory, R. Duerr, and J. Stroeve (2013), updated 2015: NOAA/NSIDC Climate Data Record of Passive Microwave Sea Ice Concentration, Version 2. Boulder, Colorado USA: National Snow and Ice Data Center [accessed 10 March 2016].

Prather, M. (1986), Numerical advection by conservation of second-order moments, Journal of Geophysical Research 91, 6671–6681.

Reynolds, R.W., N.A. Rayner, T.M. Smith, D.C. Stokes, and W. Wang (2002), An improved in situ and satellite SST analysis for climate. J. Climate, 15, 1609-1625.

Roquet, F., G. Madec, T. McDougall, and P. Barker (2015), Accurate polynomial expressions for the density and specific volume of seawater using the teos- 10 standard. Ocean Modelling, 90, 29–43.

Rousset, C., Vancoppenolle, M., Madec, G., Fichefet, T., Flavoni, S., Barthélemy, A., Benshila, R., Chanut, J., Levy, C., Masson, S., and Vivier, F. (2015), The Louvain-la-Neuve sea ice model LIM3.6: global and regional capabilities, Geosci. Model Dev. Discuss., 8, 3403-3441.

Schweiger, A., R. W. Lindsay, J. Zhang, M. Steele, H. Stern, and R. Kwok (2011), Uncertainty in modeled Arctic sea ice volume, J. Geophys. Res., 116, 1–21, doi:10.1029/2011JC007084.

Semtner, A. (1976), A model for the thermodynamic growth of sea ice in numerical investigations of climate, J. Phys. Oceanogr., 6, 379–389.

Shine, K.P., Henderson-Sellers, A. (1985), The sensitivity of a thermodynamic sea ice model to changes in surface albedo parameterization, Journal of Geophysical Research 90, 2243–2250.

Smedsrud, L. H., A. Sirevaag, K. Kloster, A. Sorteberg, and S. Sandven (2011), Recent wind driven high sea ice area export in the Fram Strait contributes to Arctic sea ice decline, Cryosph., 5(4), 821–829, doi:10.5194/tc-5-821-2011.

Steele, M., R. Morley, and W. Ermold (2001), PHC: A global ocean hydrography with a high quality Arctic Ocean, J. Climate, 14, 2079-2087.

Thorndike, A. S., D. A. Rothrock, G. A. Maykut, and R. Colony (1975), The thickness distribution of sea ice. J. Geophys. Res., 80, 4501–4513.

Timmermann, R., H. Goosse, G. Madec, T. Fichefet, C. Ethé, and V. Duliére (2005), On the representation of high latitude processes in the orcalim global coupled sea ice-ocean model. Ocean Modelling, 8:175–201.

Timmermann, R., S. Danilov, J. Schröter, C. Böning, D. Sidorenko, and K. Rollenhagen (2009), Ocean circulation and sea ice distribution in a finite element global sea ice-ocean model, Ocean Model., 27(3-4), 114–129, doi:10.1016/j.ocemod.2008.10.009.

Turner, J., J. S. Hosking, G. J. Marshall, T. Phillips, and T. J. Bracegirdle (2015), Antarctic sea ice increase consistent with intrinsic variability of the Amundsen Sea Low, Clim. Dyn., 46(7), 2391– 2402, doi:10.1007/s00382-015-2708-9.

Uppala SM, Køallberg PW, Simmons AJ, Andrae U, Da Costa Bechtold V, Fiorino M, Gibson JK, Haseler J, Hernandez A, Kelly GA, Li X, Onogi K, Saarinen S, Sokka N, Allan RP, Andersson E, Arpe K, Balmaseda MA, Beljaars ACM, Van De Berg L, Bidlot J, Bormann N, Caires S, Chevallier F, Dethof A, Dragosavac M, Fisher M, Fuentes M, Hagemann S, Hólm E, Hoskins BJ, Isaksen L, Janssen PAEM, Jenne R, McNally AP, Mahfouf JF, Morcrette J-J, Rayner NA, Saunders RW, Simon P, Sterl A, Trenberth KE, Untch A, Vasiljevic D, Viterbo P, Woollen J. (2005), The ERA-40 re-analysis. Q. J. R. Meteorol. Soc. 131: 2961–3012.

Uotila, P., T. Vihma, and J. Launiainen (2000), Response of the Weddell Sea pack ice to wind forcing, Journal of Geophysical Research, 105(C1), 1135–1151.

Uotila, P., S. P. O'Farrell, S. J. Marsland, and D. Bi, 2012: A sea-ice sensitivity study with a global ocean-ice model, Ocean Model., 1(1), 1–59.

Uotila, P., P. R. Holland, T. Vihma, S. J. Marsland, and N. Kimura (2014), Is realistic Antarctic sea-ice extent in climate models the result of excessive ice drift?, Ocean Model., 79, 33–42, doi:10.1016/j.ocemod.2014.04.004.

Vaughan, D.G., J.C. Comiso, I. Allison, J. Carrasco, G. Kaser, R. Kwok, P. Mote, T. Murray, F. Paul, J. Ren, E. Rignot, O. Solomina, K. Steffen and T. Zhang (2013), Observations: Cryosphere. In: Climate Change 2013: The Physical Science Basis. Contribution of Working Group I to the Fifth Assessment Report of the Intergovernmental Panel on Climate Change [Stocker, T.F., D. Qin, G.-K. Plattner, M. Tignor, S.K. Allen, J. Boschung, A. Nauels, Y. Xia, V. Bex and P.M. Midgley (eds.)]. Cambridge University Press, Cambridge, United Kingdom and New York, NY, USA.

Zalesak, S. T., (1979), Fully multidimensional flux corrected transport algorithms for fluids. J. Comput. Phys., 31.

Vancoppenolle, M., Fichefet, T., and Bitz, C. M. (2005), On the sensitivity of undeformed Arctic sea ice to its vertical salinity profile, Geophys. Res. Lett., 32, L16502, doi:10.1029/2005GL023427.

Vancoppenolle, M., Fichefet, T., Goosse, H., Bouillon, S., Madec, G., and Maqueda, M. A. (2009a), Simulating the mass balance and salinity of Arctic and Antarctic sea ice. 1. Model description and validation, Ocean Model., 27, 33–53.

Vancoppenolle, M., Fichefet, T., and Goosse, H. (2009b) Simulating the mass balance and salinity of Arctic and Antarctic sea ice: II. Sensitivity to salinity processes, Ocean Model., 27, 54–69.

Vancoppenolle, M., Bouillon, S., Fichefet, T., Goosse, H., Lecomte, O., Morales Maqueda, M. A., and Madec, G. (2012), The Louvain-la-Neuve sea ice model, Notes du pole de modélisation, Institut Pierre-Simon Laplace (IPSL), Paris, France, No 31 ISSN No 1288–1619.

Vancoppenolle, M., T. Fichefet, H. Goosse, S. Bouillon, and M. A. M. Maqueda (2015), LIM3, an advanced sea-ice model for climate simulation and operational oceanography, Mercator Newsletter, (8), 1–6.

Wang, Q. et al. (2016a), An assessment of the Arctic Ocean in a suite of interannual CORE-II simulations. Part I: Sea ice and solid freshwater, Ocean Model., 99, 110–132, doi:10.1016/j.ocemod.2015.12.008.

Wang, Q. et al. (2016b), An assessment of the Arctic Ocean in a suite of interannual CORE-II simulations. Part II: Liquid freshwater, Ocean Model., 99, 86–109, doi:10.1016/j.ocemod.2015.12.009.
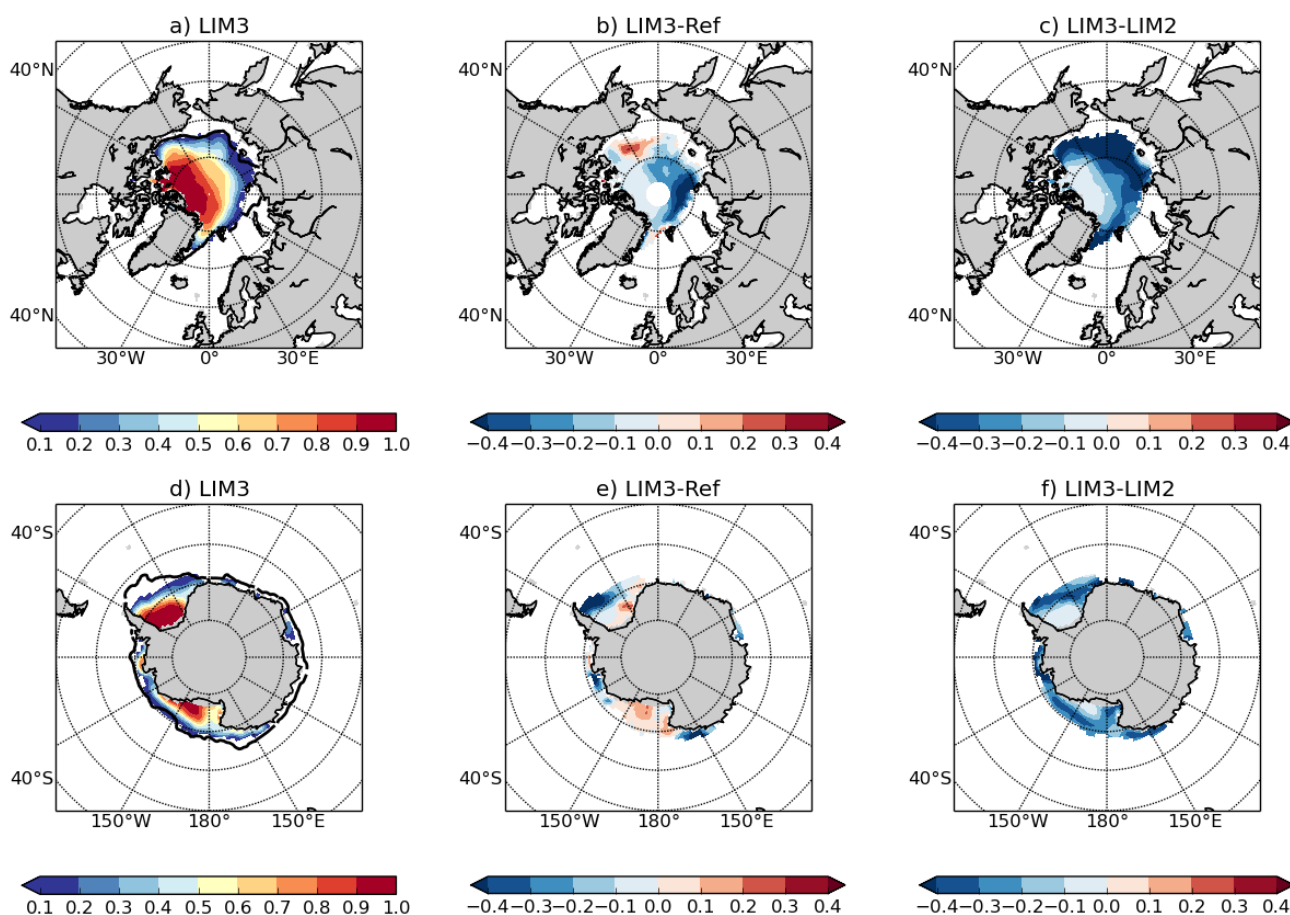
Figure 1. Geographical distribution of Arctic sea-ice concentration averaged for September (a–c) and Antarctic sea-ice concentration averaged for March 2003–2012 (d–e). (a, d) show values simulated by LIM3, while (b, e) show LIM3 difference with Meier et al. (2013) passive microwave observations and (c, f) with LIM2. Sea-ice concentration differences are computed only where both values are present. Only areas where the sea-ice concentration is greater than 15% are plotted. In (a, d), thick black lines show the observed sea-ice edge as the 15% sea-ice concentration isopleth.
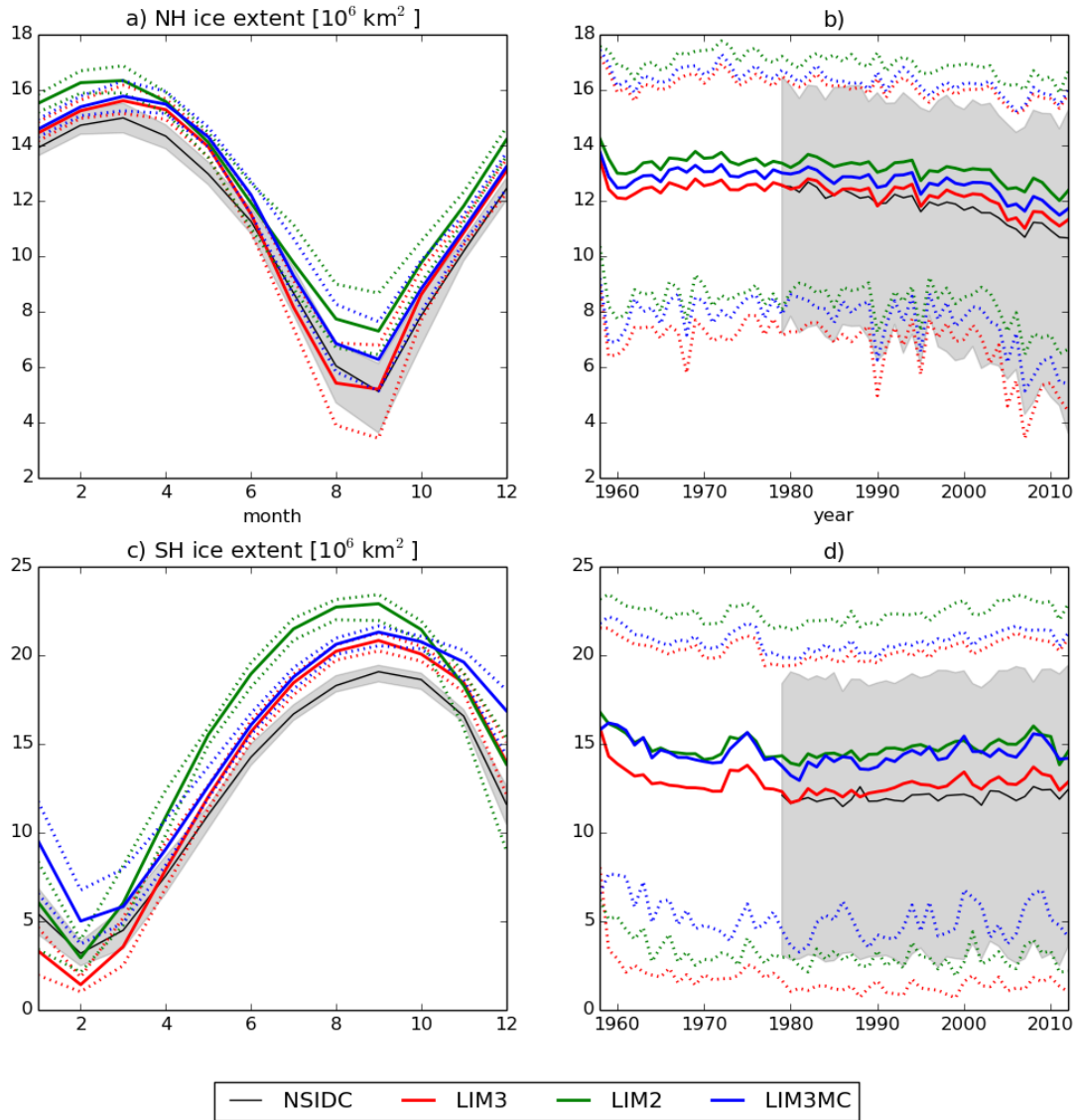
Figure 2. Simulated (coloured lines) and observed (black lines and grey shadings; NSIDC Fetterer et al., 2002) mean seasonal cycle (a, c) of monthly mean sea-ice extent over the period 2003–2012, for the (a) northern (NH) and (c) southern (SH) hemispheres. The sea-ice extent is calculated as the area with sea-ice concentration 15 % or more. Dashed lines and grey shadings denote the minimum and maximum annual monthly extents during the same period. In the rightmost panels (b, d), annual maximum, mean and minimum time series of simulated and observed sea-ice extents in (b) the NH and (d) SH over the period of 1958–2012 are presented. LIM3 (red lines) denote the reference LIM3 simulation, LIM2 (green lines) denote the reference LIM2 simulation, and LIM3MC (blue lines) denote the LIM3 single-category sea-ice simulation.
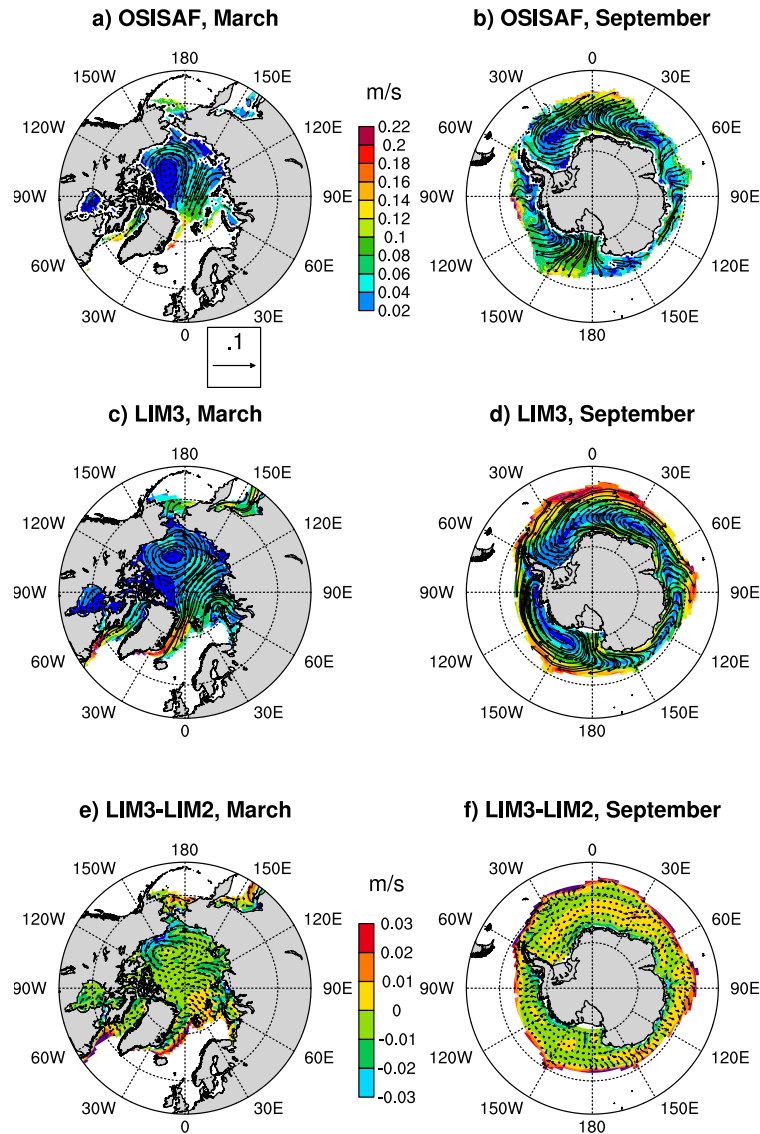
Figure 3. (a) Observed satellite-based average Arctic sea-ice velocity in March (Lavergne et al., 2010) as arrows and the corresponding vector magnitude (speed, m/s) as filled coloured contours based on years 2009–2015. (b) as (a), but for the Antarctic in September and based on years 2013–2015. (c) is similar to (a), and (d) is similar to (b), but for LIM3 ice velocity and speed based on years 2003–2012. In (e), mean differences between LIM3 and LIM2 ice velocity and speed are shown in the NH in March, while (f) displays the corresponding differences in the SH in September.
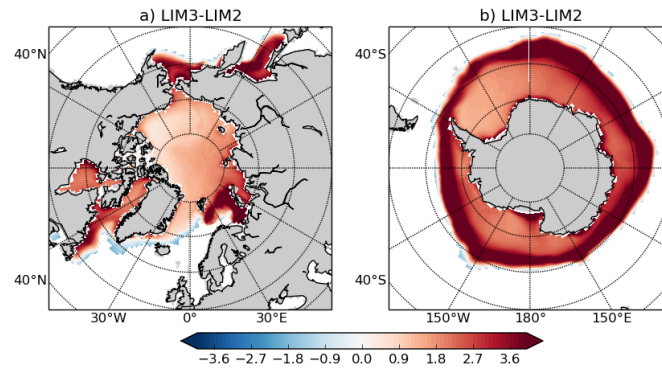
Figure 4. The sea-ice salinity difference (in ppm) between LIM3 and LIM2 (a) in the Arctic in March and (b) in the Antarctic in September. Note that the LIM2 sea-ice salinity is constant 4 ppm.
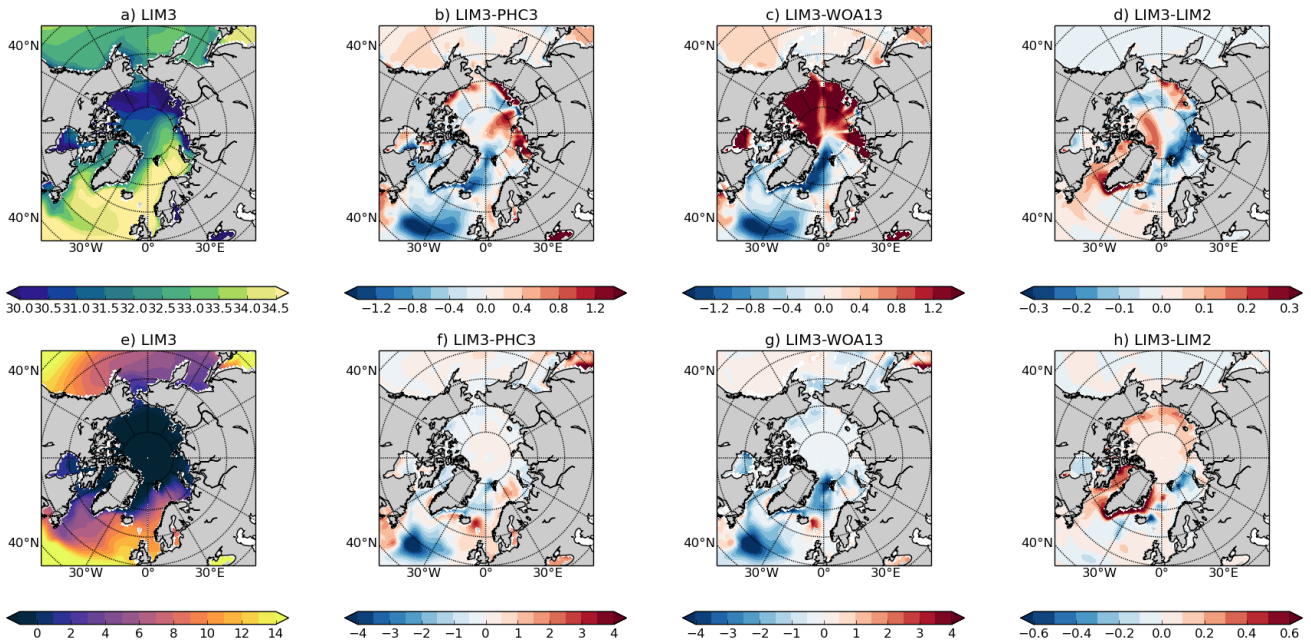
Figure 5. (a–d) Arctic sea-surface salinity in psu (SSS) and (e–h) sea-surface temperature in °C (SST) averaged over the period of 2003–2012. (a, e) show the LIM3 averages, (b, f) the difference between PHC3 (Steele et al., 2001) and LIM3, (c, g) the difference between WOA13 (Boyer et al., 2013) and LIM3, and (d, h) show the difference between LIM3 and LIM2. WOA13 data are averaged over the years 2005–2013, while PHC3 data contain observations from 1900–1998, as in WOA98, plus all Arctic observations until 2004.
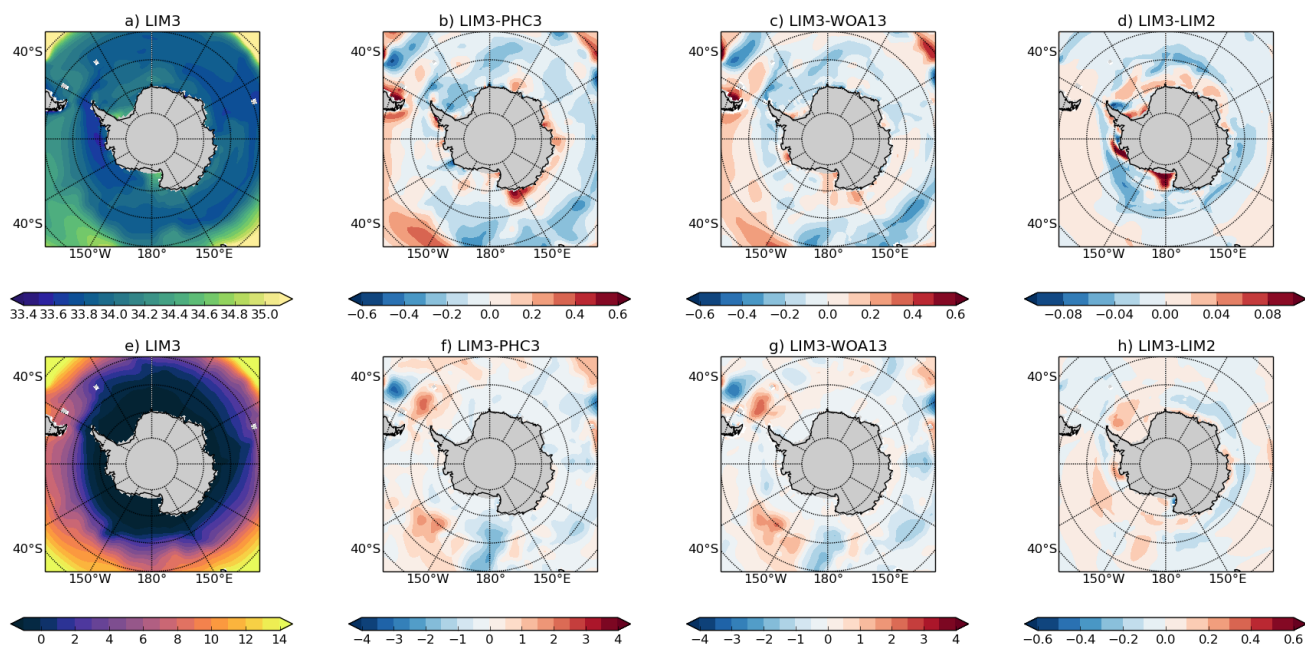
Figure 6. As Figure 5, but for the Southern Hemisphere.
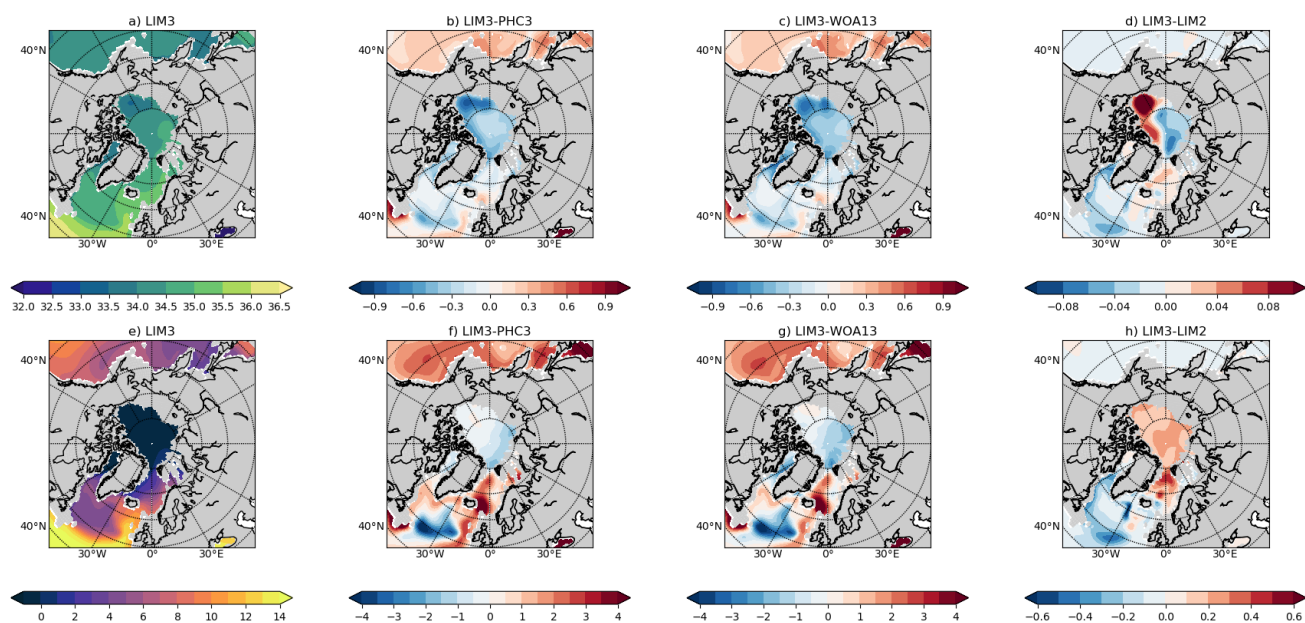
Figure 7. As Figure 5, but for the Arctic Intermediate Water (AIW) at 250 m.
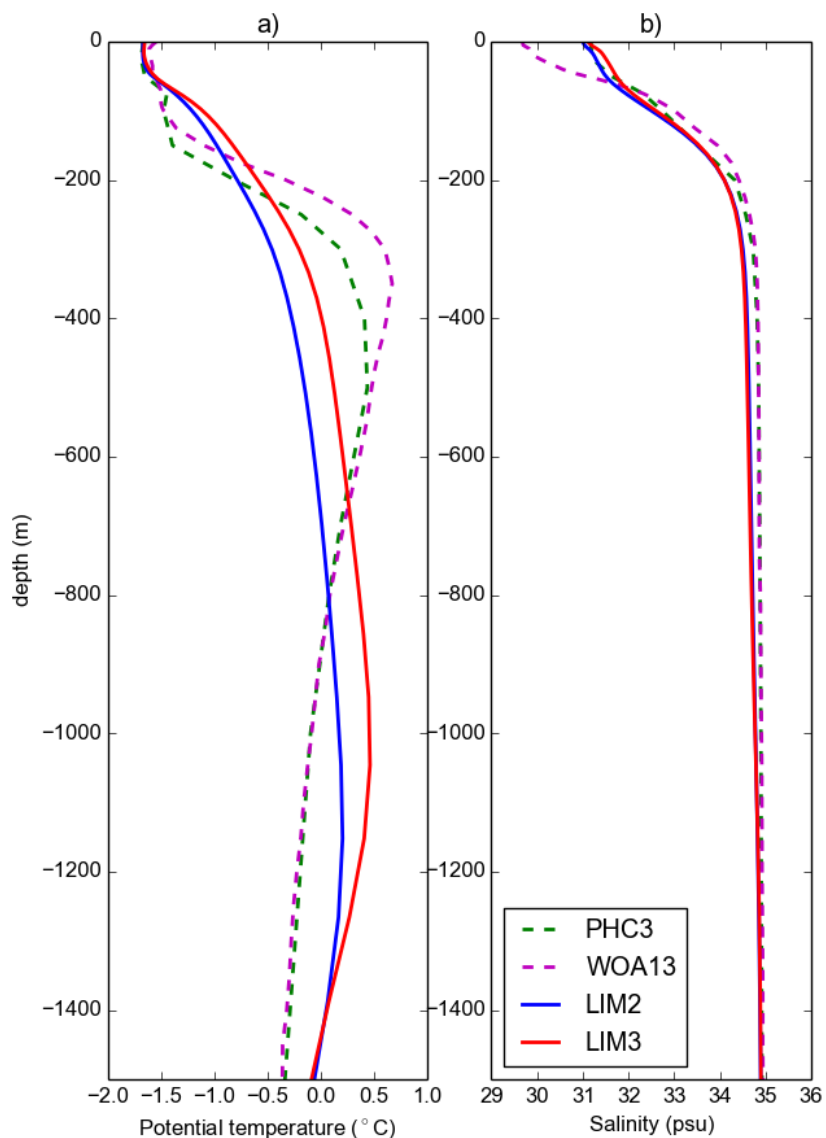
Figure 8. Vertical profiles of (a) potential temperature (°C) and (b) salinity (psu) at a grid point close to the North Pole (85.5°N, 140°W). Green dashed lines are based on the PHC3 climatology by Steele et al. (2001), magenta dashed lines are based on the WOA13 2005–2012 climatology by Boyer et al. (2013), blue lines show values from the NEMO-LIM2 simulation and red lines from the NEMO-LIM3 simulation. NEMO-LIM profiles are averages over the years 2003–2012. Note that the PHC3 data were used to initialise two NEMO-LIM simulations, after which they largely lost their initially warm Atlantic Intermediate Water.
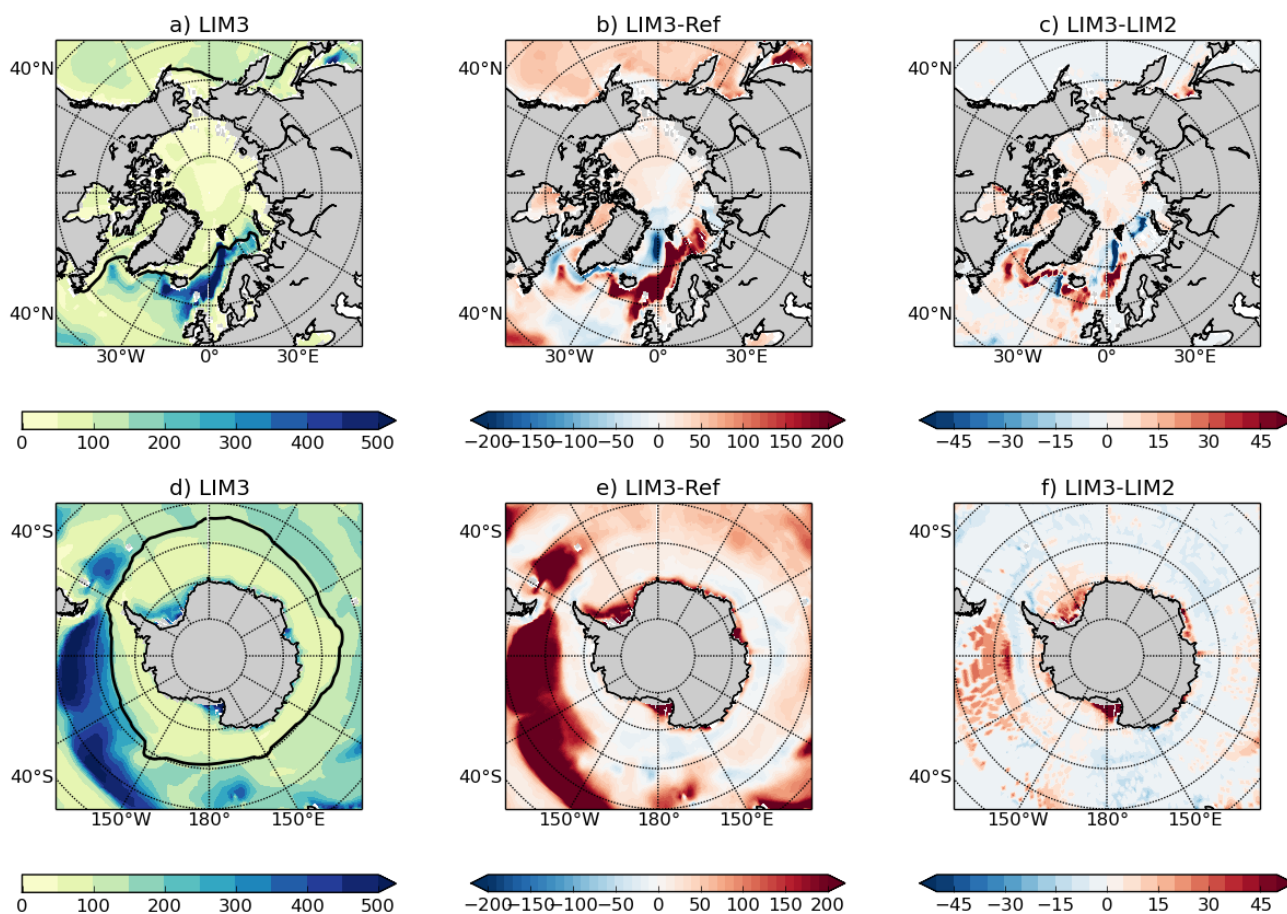
Figure 9. (a, d) mixed layer depths (in metres) as simulated by NEMO-LIM3, their departure from the observed climatology of de Boyer Montégut et al. (2004) (b, e) and differences between LIM3 and LIM2 (c, f). Top row plots represent March averages in the Northern Hemisphere (NH) and bottom row plots present September averages in the Southern Hemisphere (SH). Monthly averages were calculated from 2003–2012. Mixed layer depths are based on the potential density threshold value difference of 0.03 kg m^{-3} from the density value at 10 m depth. In (a, d), thick black lines show the observed sea-ice edge as the 15% isopleth of Meier et al. (2013) sea-ice concentration.
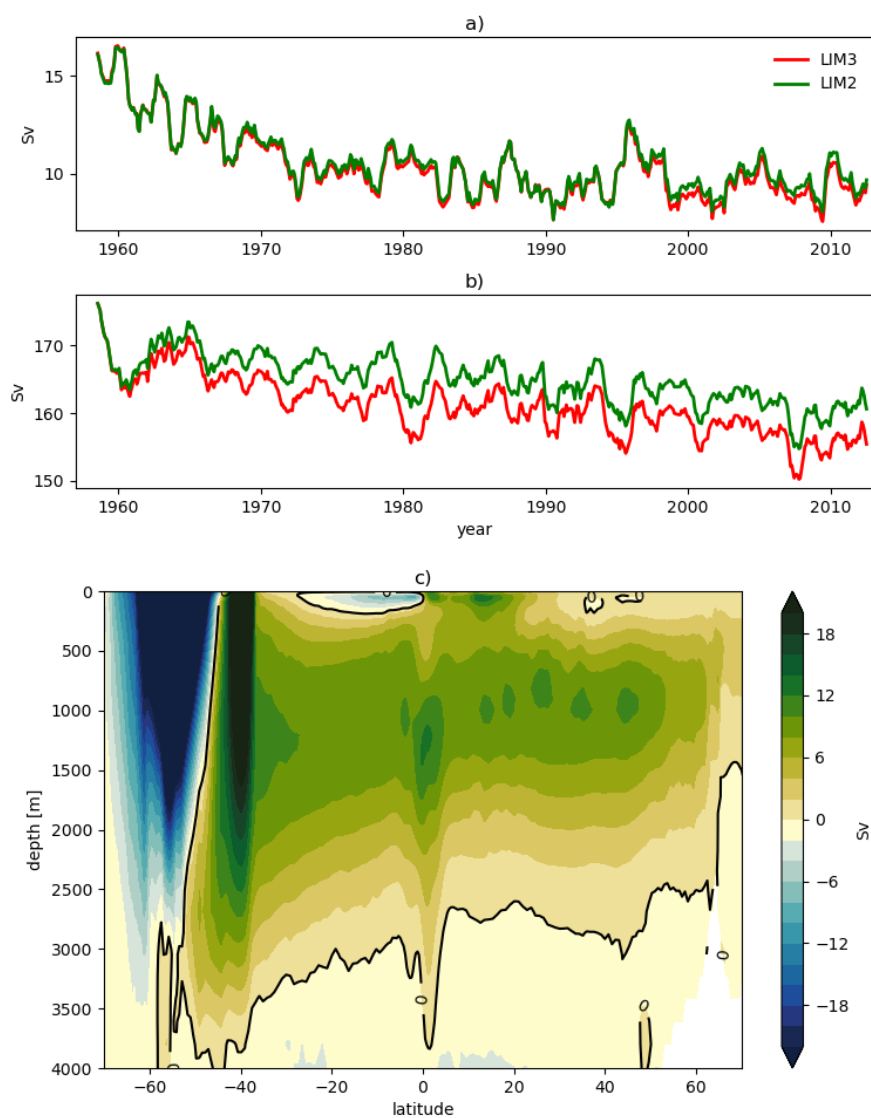
Figure 10. (a) Time series of the Atlantic Meridional Overturning Circulation (AMOC) in Sverdrups (Sv = 10^6 m^3 s^{-1}) for NEMO-LIM3 simulation (red line) and NEMO-LIM2 simulation (green line) integrated zonally across the Atlantic along the 50–53°N latitudinal band. In (b) the corresponding volume transport time series through the Drake Passage are shown. Time series in (a) and (b) represent 12 month running means. In (c), the Atlantic meridional transect of MOC (in Sv) for the NEMO-LIM3 simulation averaged over 2003–2012 as a function of depth and latitude is presented.